Title

Influence of Temperature on the Volume Change Behavior of Saturated Sand

Journal

Geotechnical Testing Journal, 41(4)

ISSN

0149-6115

Authors

Liu, Hong
Liu, Hanlong
Xiao, Yang
et al.

Publication Date

2018-07-01

DOI

10.1520/gtj20160308

Peer reviewed

Influence of temperature on the volume change behavior of saturated sand

Journal:	*Geotechnical Testing Journal*
Manuscript ID	GTJ-2016-0308.R3
Manuscript Type:	Technical Manuscript
Date Submitted by the Author:	07-Sep-2017
Complete List of Authors:	Liu, Hong; Chongqing University Liu, Hanlong; Chongqing University Xiao, Yang McCartney, John; University of California San Diego, Department of Structural Engineering
ASTM Committees and Subcommittees:	D18.05 Strength and Compressibility of Soils < D18 Committee on Soil and Rock
Keywords:	energy geostructures, axial strain, volumetric strain, pore water, soil skeleton
Abstract:	The effect of temperature on the volume change of sand is rarely reported but may be relevant to the performance of energy geostructures. This study involves an investigation of the thermal volume change behavior of saturated, dense sand through a series of temperature-controlled, isotropic hollow cylinder triaxial compression tests. Variables measured during a heating stage include the volume of water expelled from the sand specimen, the temperatures at the top, bottom, and inside of the specimen, the axial and volumetric strains. The volumes were used along with thermo-elastic relationships for the pore water and soil skeleton to infer the axial and volumetric strains during drained heating. It was observed that the thermally-induced axial and volumetric strains were negative, reflecting expansion. The pore water was observed to flow out of the sand specimen during heating, reflecting differential thermal expansion of the pore water and sand particles. The thermal volume changes were observed to be independent of the mean effective stress, as the dense sand specimens were all in normally consolidated conditions. Three linear equations incorporating the effects of temperature on the volume change behavior of dense sand were proposed and match well with the experimental data. The experimental approach proposed in this study can be used in the future to evaluate the role of sand density and stress state on the parameters of these equations.

Influence of temperature on the volume change behavior of saturated sand

Hong Liu[1], Hanlong Liu [2], Yang Xiao[3], John S. McCartney[4]

1. Hong Liu

Ph.D. Candidate, School of Civil Engineering, Chongqing University, Chongqing, 400450, China. E-mail: cqulhong@163.com

2. Hanlong Liu

Professor and Chair, School of Civil Engineering, Chongqing University, Chongqing, 400450, China. E-mail: cehliu@hhu.edu.cn

3. Yang Xiao (Corresponding author)

Associate Professor, China Key Laboratory of New Technology for Construction of Cities in Mountain Area (Chongqing University), Ministry of Education, Chongqing, 400045, China; Associate Professor, School of Civil Engineering, Chongqing University, Chongqing, 400450, China. E-mail: hhuxyanson@163.com

4. John S. McCartney, Ph.D., P.E.

Associate Professor, Department of Structural Engineering, University of California San Diego, 9500 Gilman Drive, La Jolla, CA, 92093-0085, USA. Email: mccartney@ucsd.edu

Abstract: The effect of temperature on the volume change of sand is rarely reported but may be relevant to the performance of energy geostructures. This study involves an investigation of the thermal volume change behavior of saturated, dense sand through a series of temperature-controlled, isotropic hollow cylinder triaxial compression tests. Variables measured during a heating stage include the volume of water expelled from the sand specimen, the temperatures at the top, bottom, and inside of the specimen, the axial and volumetric strains. The volumes were used along with thermo-elastic relationships for the pore water and soil skeleton to infer the axial and volumetric strains during drained heating. It was observed that the thermally-induced axial and volumetric strains were negative, reflecting expansion. The pore water was observed to flow out of the sand specimen during heating, reflecting differential thermal expansion of the pore water and sand particles. The thermal volume changes were observed to be independent of the mean effective stress, as the dense sand specimens were all in normally consolidated conditions. Three linear equations incorporating the effects of temperature on the volume change behavior of dense sand were proposed and match well with the experimental data. The experimental approach proposed in this study can be used in the future to evaluate the role of sand density and stress state on the parameters of these equations.

Keywords: energy geostructures; axial strain; volumetric strain; pore water; soil skeleton

Introduction

In recent years, interest in the thermo-mechanical behavior of soils has grown due to analyses involved in the design of nuclear waste repositories (Gens et al. 2009), trenches for high voltage electric cables (Sun et al. 2011), energy piles (Brandl 2006; Knellwolf et al. 2011; Ma and Grabe 2010; Olgun and McCartney 2014), highway pavements (Bianchini et al. 2011; Kertesz and Sansalone 2014) and geothermal structures (Brandl 2006; Stewart et al. 2014). The thermal volume change of saturated or unsaturated clays and silts have been investigated in several studies (Baldi et al. 1988; Burghignoli et al. 2000; Coccia and McCartney 2016a; Kuntiwattanakul et al. 1995; Ng and Zhou 2014; Romero et al. 2005; Uchaipichat and Khalili 2009; Vega and McCartney 2015; Zhou and Ng 2016). The thermal volume change of clays and silts have been observed to depend on variables such as stress history (Baldi et al. 1988; Cekerevac and Laloui 2004; Graham et al. 2001; Sultan et al. 2002; Abuel-Naga, 2006; Coccia and McCartney 2016b; Coccia and McCartney 2016c), degree of saturation (Alsherif and McCartney 2015; Uchaipichat and Khalili 2009), rate of heating (Vega et al. 2012), drainage conditions (Kuntiwattanakul et al. 1995; Takai et al. 2016), cyclic heating and cooling (Ng and Zhou 2014; Vega and McCartney 2015) and anisotropy (Coccia and McCartney 2011; Shamy et al. 2013; Wang et al. 2016). However, only limited studies have been performed to evaluate the impact of different variables on the thermal volume change of sands (Agar et al. 1986; Demars and Charles 1982; Ng et al. 2016). This is an important gap in the literature as sands are frequently encountered in geotechnical applications that may undergo temperature changes.

An early study on the thermo-mechanical behavior of different soils including sand was

performed by Demars and Charles (1982). Specifically, they performed a series of isotropic triaxial compression tests on clays, silts, clayey silts and sand to investigate the permanent volume deformations of natural marine soils undergoing a heating and cooling cycle with a change in temperature of 25 °C. They found that the permanent volume deformation due to the temperature cycle was independent of the mean effective stress, and ranged from no measurable volumetric strain for sand to a contractile volumetric strain of 1.80% for clay. The lack of measureable thermal volume change for sand may due to the limitations of the experimental instruments available at the time, which experienced temperature variations of ±2 °C during testing, and the heating rate (0.7 °C/min) was relatively fast and may have led to drainage issues even in dense sands. Ng et al. (2016) observed that loose specimens (i.e., relative density of D_r = 21%) and medium-dense specimens (i.e., D_r = 70%) of Toyoura sand contracted as the temperature increased from 23 °C to 35 °C, but expanded as the temperature increased up to 50 °C. However, they observed that dense specimens (i.e., D_r = 90%) of Toyoura sand showed only expansion. The volume of water expelled out of the loose specimen measured by backpressure volume control was observed to be greater than the theoretical thermal expansion values of the pore water and solid skeleton of the specimen, and the specimen was observed to contract volumetrically during heating. For denser sand specimens, the theoretical thermal expansion values of the pore water and solid skeleton of the specimens increased so that they were greater than the volume of water expelled during heating. This change resulted in a transition from contractive to expansive behavior during heating with increasing relative density.

In most of the studies on the thermal volume change of different soils mentioned above,

the soil specimens investigated in the temperature-controlled tests are usually solid and cylindrical in shape, with a maximum diameter and height of 61.8 and 125 mm, respectively. These dimensions are large enough where a temperature gradient may occur between the interior and surface of the specimens during transient heating or temperature cycling, and may result in a inhomogeneous temperature distribution throughout the specimens if full equilibrium is not reached. Although the hollow cylinder test is conventionally used to study more complex stress paths than in the triaxial apparatus, the geometry of a hollow cylinder soil specimen may be advantageous for thermal volume change measurements as temperature changes can be applied to both the inside and outside of the specimen to reach more uniform temperature distributions.

The main objective of this paper is to evaluate the thermal volume change behavior of saturated sand specimens under isotropic stress states by conducting a number of temperature-controlled hollow triaxial tests. Variables measured include the water volume expelled out of the specimens as well as axial and volumetric strains during drained heating. In addition, the influences of temperatures and mean effective stresses on axial and volumetric strains of sand are also described.

Test apparatus

Fig. 1 shows a photo of the temperature-controlled hollow triaxial apparatus. The apparatus includes four parts (i.e., pressure control panel, load cell, pressure cell and temperature control system) and was modified from a computer-controlled hollow-cylinder triaxial testing system developed to evaluate frozen soils obtained from Geotechnical Consulting and Testing

Systems (GCTS) of Phoenix, AZ. The major addition to this system is the addition of a temperature control system that can apply temperatures to the boundaries of the soil specimen ranging from -20 to +80 °C.

The temperature control system consists of an oil bath, a heater, a circulating pump, a heat exchanger in the metal cover of the outer cell in a spiral loop configuration, a heat exchanger in the inner cell in a "U"-loop configuration, and three temperature sensors (T1, T2 and T3) in different locations as shown in Figure 2. The temperature sensors are model Pt100 obtained from GCTS of Phoenix, AZ. To control the temperature, a heat exchange fluid is circulated through the closed-loop metal tubing on the outside and inside of the cell. The heat exchange fluid is an oil that can be used at different temperatures (model thermal C5 obtained from Julabo GmbH of Seelbach, Germany), and its temperature was controlled using a heating unit with an internal circulating pump.

Temperature sensors T1 and T2 were placed in the outer cell to measure the temperature near the bottom and top of the specimen, respectively. The average of the values measured by temperature sensors T1 and T2 was referred to as the outer temperature. Temperature sensor T2 was used to provide feedback to the thermostat in the oil bath for setting the target temperature applied to the specimen. The thermostat in the oil bath controls the power supplied to the heating unit until thermal equilibrium between the measured and target temperatures was reached. Temperature sensor T3 was used to measure the inner temperature of the specimen, which can be used to evaluate the distribution in temperature throughout the thickness of the hollow cylinder specimen.

Testing program

Temperature-controlled hollow triaxial tests were conducted on reconstituted specimens of sand (Xiao et al. 2017a) from Fujian, China. As shown in Fig. 3, the sand has a mean grain size D_{50} of 0.60 mm, a coefficient of uniformity C_u of 7.05, a coefficient of curvature C_c of 0.54. The maximum and minimum void ratios are 0.708 (ASTM 2014a) and 0.335 (ASTM 2014b), respectively. This sand is a standard sand in China with more than 96% SiO_2, and is used widely in geotechnical laboratory experiments (Xiao et al. 2017b).

The outer diameter, inner diameter and height of the specimens are 100 mm, 60 mm, 200 mm, respectively. The sand specimens were prepared by placing predetermined quantities of soil in the mold filled with de-aired water (Wanatowski and Chu 2008), and gently compacting it in eight layers using a flat-bottom tamper to reach a relative density D_r of approximately 90% corresponding to a dense state.

The details of the experimental program are presented in Table 1. In order to seal the neoprene membranes, two pairs of thermally resistant Viton O-rings (obtained from GCTS of Phoenix, AZ) were placed around the pedestal and top cap of the inner and outer cells, respectively.

Once the specimen was set up in the cell, the outer stress p_o and inner stress p_i were applied ($p_o = p_i$), and it was ensured that the differences between the outer/inner stresses and the backpressure stress were below 20 kPa. Then, the backpressure stress u_w and outer/inner stresses were increased as a slow rate of 50 kPa/h until reaching an appropriate B-value reflecting saturated conditions. For all specimens, the Skempton's B-values were measured to be greater than 0.95 at the end of backpressure saturation. Figure 4 shows the stress paths for

Fujian sand. After saturation, all specimens were isotropically consolidated to mean effective stresses of p' = 50, 100, 200 kPa by raising the outer and inner stresses to different values ($p_o = p_i = \sigma_3$ = 350, 400, 500 kPa) while keeping the back stress u_w constant at 300 kPa under a constant temperature of 25 °C (i.e., path from 0 to 1). The axial stress was also controlled to be the same as the inner and outer stresses during this process, corresponding to an isotropic stress state. While maintaining the axial, outer, inner and backpressure stresses of the specimens constant, the specimens were heated in drained conditions to different target values at a rate of 5 °C/h. For each mean effective stress, four different temperatures (T= 25, 35, 45, 55 °C) were applied (i.e., path from 1 to 2), which are within the range of temperatures experienced in energy geostructures (Murphy and McCartney 2015).

Thermal calibration test

Method

A metallic sample 100 mm in diameter and 200 mm in height was used to characterize the thermal expansion of the apparatus (e.g. the drainage system, top soil cap and axial rod), which was recommended by Cekerevac et al. (2005). The calibration test began at room temperature (25 °C) by applying the desired mean effective stress (p' = 50, 100, 200 kPa), and then followed by rising the temperature at a rate of 5 °C/h, until 65 °C. Thereafter, the temperature of the metallic sample was decreased to the room state (25 °C).

During the heating and cooling phases, the axial strain of the metallic sample is nearly reversible (as shown in Figure 5), which indicates that the thermal expansion of the top soil cap and axial rod can be neglected. The slight differences in the axial strain could be due to

slight variances in temperature distribution in the cell.

In addition, the drainage system was open during the calibration test, and volume change of the whole system ΔV_{ws} (i.e. drainage system and metallic sample) was measured by the backpressure volume controller directly, as shown in Figure 6. The results indicated that most of the volume change were reversible (i.e. ΔV_{ws}^{r}), and these variations were caused by the dilation of the metallic sample. The other volume change were irreversible (i.e. ΔV_{ws}^{ir}), and these were the change in volume of the drainage system due to temperature change. Further, these irreversible volume change were used to correct the volumetric strain of sand specimen during heating.

Actual thermal axial strain

The axial displacement is measured by a linearly-variable differential transformer (LVDT) with a maximum operating range of 100 mm and an accuracy of 0.1%. The LVDT is placed at the top of the load frame, and there is a distance about 1.5 m from the LVDT to the soil specimen, as shown in Figure 1. With such a slow heating rate (5 °C/h) and a long distance, it may be reasonable to expect that the impact of temperature on the LVDT device itself could be very small and negligible. However, changes in temperature within the cell will result in both thermal expansion of the top soil cap as well as thermal expansion of the axial rod. Therefore, a calibration test mentioned above was carried out to account for thermal expansion of the top soil cap and the axial rod, as shown in Figure 5. And this irreversible axial strain, which is resulted from the thermal expansion of the top soil cap and axial rod, is of a very small value that it can be neglected.

The actual thermal axial strain of the sand specimen is defined as follows:

$$\varepsilon_a = \frac{\Delta z}{H_0} \times 100\% \quad (1)$$

where ε_a is the axial strain of the sand specimen due to temperature changes, Δz is the axial displacement measured by a LVDT, H_0 is the initial height of the sand specimen (e.g., at the end of mechanical consolidation for the case of calculating thermal strains).

Actual thermal volumetric strain

The actual volumetric strain for a hollow cylindrical sample is defined as (Hight et al. 1983):

$$\varepsilon_v = -\frac{\Delta V}{V_0} \times 100\% \quad (2)$$

where ε_v is the actual volumetric strain, ΔV is the change in volume of the sand specimen, and V_0 is the initial volume of the specimen.

During heating, the volume change of the specimen can be separated into different components, as follows (Campanella and Mitchell 1968; Cekerevac et al. 2005):

$$\Delta V = \Delta V_{dr} - \Delta V_{de} - \Delta V_w - \Delta V_s \quad (3)$$

where ΔV_{dr} is the volume of water flowing out or into the specimen which can be measured using the backpressure volume controller. The accuracy of volume controller is 0.01 cm^3. ΔV_{de} is the thermal expansion of the drainage system, which is the irreversible component during a calibration test (i.e. $\Delta V_{de} = \Delta V_{ws}^{ir}$). ΔV_w is the thermal expansion of the pore water, and ΔV_s is the thermal expansion of the solid skeleton. The value of ΔV_w can be defined as follows:

$$\Delta V_w = \beta_w (T - T_0) V_w \quad (4)$$

where β_w is the volumetric coefficient of thermal expansion of pore water which is assumed to be a function of temperature using the relationship presented by Campanella and Mitchell (1968), T is the target temperature, T_0 is the initial ambient room temperature (25 °C), and V_w is the volume of pore water in the specimen after mechanical consolidation. The value of ΔV_s can be defined as follows:

$$\Delta V_s = \beta_s (T - T_0) V_s \quad (5)$$

where β_s is the volumetric coefficient of thermal expansion of the solid skeleton and V_s is the volume of the solid skeleton after mechanical consolidation. As the volumetric coefficient of thermal expansion of the sand investigated in this study was not directly measured in this study, a value of 3.5×10^{-5}/°C was assumed based on the range of values presented by Campanella and Mitchell (1968).

The strain values given in Equations (1)-(5) were used to interpret the actual volume changes of the hollow cylinder sand specimens during drained heating.

Test results

Volume of water expelled during heating

An example of time series of temperature inside and outside of the hollow cylinder sand specimen as well as the water expelled from the specimen is shown in Figure 7. The water expelled from the specimen was measured by the backpressure volume controller directly. The results in Figure 7 are for a sand specimen under a mean effective stress of 50 kPa. The heating phase has three stages, which are 25-35 °C, 35-45 °C and 45-55 °C, and each stage starts after temperature equilibrium under the former stage was achieved. For a temperature

increment of 10 °C in each heating stage applied at a rate of 5 °C/h, the temperature of the confining fluid measured by the sensors and water volume expelled out of specimen measured by the backpressure volume controller began to reach equilibrium after heating about 2 hours. The volume of water expelled from the specimen was observed to increase with increasing temperature due to the differential expansion of the pore fluid and the soil skeleton.

During the heating phase, the outer cell temperature, which is the average value of the measurements from temperature sensors T1 and T2, is lower than the inner cell temperature measured by temperature sensor T3 (as shown in Figs. 7 and 8(a)). The difference between these temperatures increases with increasing target temperature as shown in Fig. 9, which can be described using a linear relationship as follows:

$$T_{\mathrm{i}} - T_{\mathrm{o}} = \chi_{\mathrm{io}} + k_{\mathrm{io}} T \tag{6}$$

where T_{i} and T_{o} are the inner and outer temperatures, respectively; χ_{io} and k_{io} are constants related to the performance of the heating system. The values of the constants are listed in Table 3.

In addition, the bottom temperature measured by temperature sensor T1 is observed to be initially larger than the temperature at the top of the specimens measured by temperature sensor T2 during heating, although they reach agreement as the temperature in the cell stabilizes over time, as shown in Fig. 8(b). The difference between the bottom and top temperatures after heating for 2 hours decreases with an increase in the target temperature as shown in Fig. 9, which can be expressed by a linear equation as follows:

$$T_{\mathrm{b}} - T_{\mathrm{t}} = \chi_{\mathrm{bt}} + k_{\mathrm{bt}} T \tag{7}$$

where T_b and T_t are the temperatures of the bottom and top of the specimen, respectively, and χ_{bt} and k_{bt} are constants related to the performance of the heating system. The values of the constants are listed in Table 3.

The differences in temperature described by Equations (6) and (7) occur because a shorter heating path leads to lower energy losses under the same power of temperature control system. Nonetheless, the differences between the temperatures of the inner and outer cells and the target temperature are small enough to be assumed negligible (< 0.5 °C).

Trends in thermal strains during heating

Typical trends in the axial and volumetric strains during staged heating are shown in Figure 10. All the corresponding values used to determine the thermal volumetric strain using Equation (2) are listed in Table 2. As the soil temperature increases, the axial and volumetric strains are negative, reflecting expansion. This means that the pore water and soil skeleton expand during heating, and the pore water expands more than the soil skeleton due to its greater coefficient of thermal expansion. This calculation assumes that the water remains at the same temperature as the inside of the specimen when it flows out of the specimen, which is a reasonable assumption as most of the tubing is insulated near the experimental setup.

In addition, the total thermal volumetric strain can be classified into four components (as shown in Fig. 11). These are the measured volumetric strain due to water outflow or inflow, and the volumetric strains due to thermal expansion of the drainage system, pore water and solid skeleton of the sand specimen, respectively. The relationship between these four volumetric strain components can be defined as follows:

$$\varepsilon_{\mathrm{v}} = -\frac{\Delta V}{V_0} = -\frac{\Delta V_{\mathrm{dr}} - \Delta V_{\mathrm{de}} - \Delta V_{\mathrm{w}} - \Delta V_{\mathrm{s}}}{V_0}$$
$$= -\frac{\Delta V_{\mathrm{dr}}}{V_{\mathrm{w}}} \cdot \frac{V_{\mathrm{w}}}{V_0} + \frac{\Delta V_{\mathrm{de}}}{V_{\mathrm{w}}} \cdot \frac{V_{\mathrm{w}}}{V_0} + \frac{\Delta V_{\mathrm{w}}}{V_{\mathrm{w}}} \cdot \frac{V_{\mathrm{w}}}{V_0} + \frac{\Delta V_{\mathrm{s}}}{V_{\mathrm{s}}} \cdot \frac{V_{\mathrm{s}}}{V_0} \quad (8)$$
$$= \varepsilon_{\mathrm{vdr}} \cdot n + \varepsilon_{\mathrm{vde}} \cdot n + \varepsilon_{\mathrm{vw}} \cdot n + \varepsilon_{\mathrm{vs}} \cdot (1-n)$$

where $\varepsilon_{\mathrm{vdr}}$ is the measured volumetric strain due to water outflow or inflow, $\varepsilon_{\mathrm{vde}}$ is the volumetric strain due to the thermal expansion of the drainage system, $\varepsilon_{\mathrm{vw}}$ and $\varepsilon_{\mathrm{vs}}$ are the volumetric strains due to the thermal expansion of the pore water and solid skeleton of the specimen, respectively, and n is the initial porosity of the sand specimen (i.e., at the beginning of the heating phase).

The measured volumetric strain due to water outflow or inflow shown in Figure 11 is observed to be positive, reflecting contraction, and water is expelled out of the specimen during drained heating. The volumetric strains due to thermal deformations of the drainage system, pore water and solid skeleton of specimen are negative, reflecting expansion, and the thermal expansion of pore water is more than that of solid skeleton because of the greater volumetric coefficient of thermal expansion of the pore water than the solid skeleton.

It is also observed that the volume of water expelled from the specimen (after considering the impact of drainage system) is lower than the volume changes of the pore water and soil skeleton due to temperature changes. In this case the volumetric strain of sand specimen is less than zero, and the specimen reflects thermal expansion although the water flows out during heating.

Discussion

The axial strain is plotted as a function of average specimen temperature in Figures 12.

After reaching equilibrium at each stage of heating, a linear increase in the axial strain value is observed with increasing temperature. The mean effective stress applied in stress-controlled conditions was not observed to have a major effect on the thermal axial strain value. Similar trends are observed in the thermal volumetric strain plotted as a function of the average specimen temperature in Figure 13. The relationships between the thermal axial, volumetric strains and the ratio of the current temperature to the initial temperature (referred to as the temperature ratio), at different mean effective stress values can be represented using the following linear equations:

$$\varepsilon_a = k_{at}(T/T_0 - 1) \tag{9}$$

$$\varepsilon_v = k_{vt}(T/T_0 - 1) \tag{10}$$

where k_{at}, k_{vt} are material constants. The values of the constants are listed in Table 3.

The relation between the axial and volumetric strains due to temperature changes is shown in Figure 14, and can be expressed linearly, as follows:

$$\varepsilon_a = k_{av}\varepsilon_v \tag{11}$$

where k_{av} is material constant. The value of the constant is listed in Table 3.

An increase in the thermal volumetric strain will lead to an increase in the thermal axial strain, and this reflect that the sand specimen exists isotropic expansion during drained heating. And the simulation resulting from the current equation is in good agreement with the experiment data of dense sand specimens during heating to different temperatures under different mean effective stresses.

A relationship between the thermal volumetric strain and temperature can be given as follows:

$$\varepsilon_{\mathrm{v}} = \beta\left(T - T_0\right) \tag{12}$$

where β is the bulk volumetric coefficient of thermal expansion of the sand specimen (i.e., the slope in Fig. 15). The value of β is listed in Table 3.

The sign of β in this study is negative, which indicates that the dense sand specimen occurs expansion during heating. A series of β values can be obtained by the experiments performed by Ng et al. (2016) and Cekerevac et al. (2004) in a similar way. The relationship between the bulk volumetric coefficient of thermal expansion of soil and the relative densities D_{r} and overconsolidation ratio are essentially linear (as shown in Figure 16) and can be expressed by the following equations:

For sand:

$$\beta = a + bD_{\mathrm{r}} \tag{13}$$

For clay:

$$\beta = c + d(\mathrm{OCR} - 1) \tag{14}$$

where OCR is the overconsolidation ratio; a, b, c and d are material constants. The values of the constants are listed in Table 3.

It can be clear to see that with an increase in the relative density for sand (as shown in Figure 16(a)), the bulk thermal expansion coefficient β increases. And the sand specimen changes from contractive to expansive behavior. A similar relationship can be found for clay (as shown in Figure 16(b)). These results may indicate that the thermal expansive behavior increases with increasing relative density for sand or OCR for clay, and the value of β for sand is lower than that for clay, which means sand is less sensitive than clay due to temperature changes.

In addition, Ng et al. (2016) found out that a higher stress would lead to a larger change in volume of sand specimen due to temperature changes. However, this behavior was not observed in this study. This difference may be caused by the different relative density of sand. The relative density of sand specimens for the various confining stresses (p'=50, 200 kPa) in Ng et al. (2016) was 21%, and this D_r was the value prior to the thermal cycle, not the initial value. It could be observed that the initial void ratio of sand specimen at a higher mean effective stress (p'=200 kPa) was larger than that at a lower mean effective stress (p'=50 kPa) for the same relative density before heating (i.e. at the end of the mechanical consolidation phase). As we know that a looser sand always has larger contractive volumetric strain under heating (Ng et al. (2016)). Therefore, larger thermal volumetric contraction was observed when loose specimens (D_r=21%) were tested under higher mean effective stresses in Ng et al. (2016).

Further, a larger mean effective stress may result in a larger volume of pore water expelled during the mechanical consolidation phase for a loose sand specimen. Then, the expansion of pore water in sand specimen during heating phase calculated by Equation (4) is smaller, and will lead to a larger volume change of the sand specimen calculated by Equation (3). While this relationship, which is the thermal volumetric strain increases with an increase in the mean effective stress found by Ng et al. (2016), is less and less clear with an increase in the initial relative density. For a dense sand specimen, especially for relative density of 90% in this study, the relative densities at initial state are close to that after mechanical consolidation phase as shown in Figure 17. The pore water expelled from the sand specimen during mechanical consolidation phase have not evident difference at various mean effective stresses.

As a result is that the following thermal volumetric strains are close to each other for different mean effective stresses.

In all cases, the trends in the axial and volumetric strains were linear with changes in temperature. Further, the mean effective stress was not observed to have a major impact on the thermally-induced strains. Although some minor differences were noted in the thermally-induced strains for the specimens under different mean effective stresses, these were assumed to be due to minor differences in the preparations of the specimen rather than effects of the mean effective stress.

Conclusions

A series of temperature-controlled hollow triaxial tests were carried out to investigate the thermal volume change of saturated, dense sand. The water volume expelled from the sand specimens along with the axial and volumetric strains were observed to be linearly dependent on the changes in temperature. In addition, the axial and volumetric strains due to temperature changes are negative, reflecting expansion. Water was observed to flow out of the specimens during drained heating due to differential expansion of the pore water and the soil skeleton. The relationships among axial and volumetric strains were well-represented by fitted linear equations. Further research is needed to evaluate the impacts of sand density on these relationships.

Acknowledgments

The authors would like to acknowledge the financial support from the Project supported by

the National Natural Science Foundation of China (Grant No. 51678094 and Grant No. 51509024) and the Project funded by China Postdoctoral Science Foundation (Grant No. 2016M590864).

Notation

The following symbols are used in this paper:

e_0 = Initial void ratio;

ε_a =Axial strain (%);

ε_v = Volumetric strain (%);

ε_{vdr} = Measured volumetric strain due to water outflow (%);

ε_{vdr} = Volumetric strain due to thermal expansion of drainage system (%);

ε_{vw} = Volumetric strain due to thermal expansion of pore water (%);

ε_{vs} = Volumetric strain due to thermal expansion of solid skeleton (%);

n =Initial porosity of the specimen (mm);

Δz =Axial displacement (mm);

H_0 = Initial height of the specimen (mm);

V_0 = Initial volume of the specimen (cm^3);

ΔV = Change in volume of the sand specimen during heating (cm^3);

ΔV_{dr} = Volume of water flowing out or into the specimen (cm^3);

ΔV_{de} = Thermal expansion of the drainage system (cm^3);

ΔV_w = Thermal expansion of the pore water (cm^3);

ΔV_s = Thermal expansion of the solid skeleton (cm^3);

ΔV_{ws} = Thermal volume change of the whole system (cm^3);

ΔV_{ws}^{r} = Thermal volume change of the metallic specimen (cm^3);

ΔV_{ws}^{ir} = Thermal volume change of the drainage system (cm^3);

β_w = Volumetric coefficient of thermal expansion of pore water;

β_s = Volumetric coefficient of thermal expansion of solid skeleton;

V_w =Volume of pore water in the specimen after mechanical consolidation (cm^3);

V_s =Volume of the solid skeleton after mechanical consolidation (cm^3);

T = Target temperature (°C);

T_0 = Initial ambient room temperature (°C);

T_i = Inner temperature (°C);

T_o = Outer temperature (°C);

T_b = Bottom temperature (°C);

T_t = Top temperature (°C);

D_{50} =Mean grain size (mm);

C_u =Coefficient of uniformity;

C_c =Coefficient of curvature;

p' = Mean effective stress (kPa);

D_r =Relative density (%);

p_o =Outer stress (kPa);

p_i =Inner stress (kPa);

u_w =Backpressure stress (kPa);

σ_3 = Minor principal stress (kPa);

t= Heating time (h);

β = Bulk volumetric coefficient of thermal expansion of the sand specimen (%/°C);

OCR = Overconsolidation ratio;

χ_{io}, k_{io}, χ_{bt}, k_{io}, k_{bt}, k_{bt}, χ_{io}, χ_{bt}, k_{at}, k_{vt} and k_{av}, a, b, c and d =Constants.

References

Agar, J. G., Morgenstern, N. R. and Scott, J. D., 1986, "Thermal Expansion and Pore Pressure Generation in Oil Sands," *Canadian Geotechnical Journal*, Vol. 23, pp. 327-333.

Alsherif, N. A., and McCartney, J. S., 2015, "Thermal behavior of compacted silt at low degrees of saturation," *Geotechnique*, Vol. 65, No. 9, pp. 703-716.

ASTM D4253, 2014a, "Standard: Standard Test Methods for Maximum Index Density and Unit Weight of Soils Using a Vibratory Table," *Annual Book of ASTM Standards*, ASTM International , West Conshohocken, PA, pp. 1-14.

ASTM D4254, 2014b, "Standard: Standard Test Methods for Minimum Index Density and Unit Weight of Soils and Calculation of Relative Density," *Annual Book of ASTM Standards*, ASTM International , West Conshohocken, PA, pp. 1-9.

Baldi, G., Hueckel, T. and Pellegrini, R., 1988, "Thermal Volume Changes of the Mineral-Water System in Low-Porosity Clay Soils," *Canadian Geotechnical Journal*, Vol. 25, pp. 807-825.

Bianchini, A., Heitzman, M. and Maghsoodloo, S., 2011, "Evaluation of Temperature Influence on Friction Measurements," *Journal of Transportation Engineering*, Vol. 137, No. 9, pp. 640-647.

Brandl, H., 2006, "Energy Foundations and Other Thermo-Avtive Ground Structures," *Geotechnique*, Vol. 56, No. 2, pp. 81-122.

Burghignoli, A., Desideri, A. and Miliziano, S., 2000, "A Laboratory Study on the Thermomechanical Behaviour of Clayey Soils," *Canadian Geotechnical Journal*, Vol. 37, pp. 764-780.

Campanella, R. G., and Mitchell, J. K., 1968, "Influence of temperature variations on soil behaviour," *Journal of the Soil Mechanics and Foundation Division*, Vol. 94, No. 3, pp. 709-734.

Cekerevac, C. and Laloui, L., 2004, "Experimental Study of Thermal Effects on the Mechanical Behaviour of a Clay," *International Journal for Numerical and Analytical Methods in Geomechanics*, Vol. 28, No. 3, pp. 209-228.

Cekerevac, C., Laloui, L. and Vulliet, L., 2005, "A Novel Triaxial Apparatus for Thermo-Mechanical Testing of Soils," *Geotechnical Testing Journal*, Vol. 28, No. 2, pp. GTJ12311.

Coccia, C. J. R. and McCartney, J. S., 2011, "A Thermo-Hydro-Mechanical True Triaxial Cell for Evaluation of the Impact of Anisotropy on Thermally Induced Volume Changes in Soils," *Geotechnical Testing Journal*, Vol. 35, No. 2, pp. 1-11.

Coccia, C. J. R. and McCartney, J. S., 2016a, "High-Pressure Thermal Isotropic Cell for Evaluation of Thermal Volume Change of Soils," *Geotechnical Testing Journal*, Vol. 39, No. 2, pp. 217-234.

Coccia, C. J. R. and McCartney, J. S., 2016b, "Thermal Volume Change of Poorly Draining Soils I: Critical Assessment of Volume Change Mechanisms," *Computers and Geotechnics*, Vol. 80, pp. 26-40.

Coccia, C. J. R. and McCartney, J. S., 2016c, "Thermal Volume Change of Poorly Draining Soils Ii: Model Development and Experimental Validation," *Computers and Geotechnics*, Vol. 80, pp. 16-25.

Demars, K. R. and Charles, R. D., 1982, "Soil Volume Changes Induced by Temperature

Cycling," *Canadian Geotechnical Journal*, Vol. 19, pp. 188-194.

Gens, A., Sánchez, M., Guimarães, L. D. N., Alonso, E. E., Lloret, A., Olivella, S., Villar, M. V. and Huertas, F., 2009, "A Full-Scale in Situ Heating Test for High-Level Nuclear Waste Disposal: Observations, Analysis and Interpretation," *Géotechnique*, Vol. 59, No. 4, pp. 377-399.

Graham, J., Tanaka, N., Crilly, T. and Alfaro, M., 2001, "Modified Cam-Clay Modelling of Temperature Effects in Clays," *Canadian Geotechnical Journal*, Vol. 38, No. 3, pp. 608-621.

Hight, D. W., Gens, A., and Symes, M. J., 1983, "The Development of a New Hollow Cylinder Apparatus for Investigating the Effects of Preincipal Stress Rotation in Soils," *Geotechnique*, Vol. 33, No. 4, pp. 355-383.

Kertesz, R. and Sansalone, J., 2014, "Hydrologic Transport of Thermal Energy from Pavement," *Journal of Environmental Engineering*, Vol. 140, No. 8, pp. 04014028.

Knellwolf, C., Peron, H. and Laloui, L., 2011, "Geotechnical Analysis of Heat Exchanger Piles," *Journal of Geotechnical and Geoenvironmental Engineering*, Vol. 137, No. 10, pp. 890-902.

Kuntiwattanakul, P., Towhata, I., Ohishi, K. and Seko, I., 1995, "Temperature Effects on Undrained Shear Characteristics of Clay," *Soils and Foundations*, Vol. 35, No. 1, pp. 147-162.

Ma, X. and Grabe, J., 2010, "Field Test of a Geothermal System in Hafencity Hamburg," *Geoenvironmental Engineering and Geotechnics*, No. 204, pp. 159-166.

Murphy, K. D. and McCartney, J. S., 2015, "Seasonal Response of Energy Foundations During Building Operation," *Geoenvironmental and Geological Engineering*, Vol. 33, No. 2,

pp. 343-356.

Ng, C. W. W., Wang, S. H. and Zhou, C., 2016, "Volume Change Behaviour of Saturated Sand under Thermal Cycles," *Géotechnique Letters*, Vol. 6, No. 2, pp. 124-131.

Ng, C. W. W. and Zhou, C., 2014, "Cyclic Behaviour of an Unsaturated Silt at Various Suctions and Temperatures," *Géotechnique*, Vol. 64, No. 9, pp. 709-720.

Olgun, C. G. and McCartney, J. S., 2014, "Outcomes from International Workshop on Thermoactive Geotechnical Systems for near-Surface Geothermal Energy: From Research to Practice," *DFI Journal - The Journal of the Deep Foundations Institute*, Vol. 8, No. 2, pp. 59-73.

Romero, E., Villar, M. V. and Lloret, A., 2005, "Thermo-Hydro-Mechanical Behaviour of Two Heavily Overconsolidated Clays," *Engineering Geology*, Vol. 81, No. 3, pp. 255-268.

Shamy, U. E., Leon, O. D. and Wells, R., 2013, "Discrete Element Method Study on Effect of Shear-Induced Anisotropy on Thermal Conductivity of Granular Soils," *International Journal of Geomechanics*, Vol. 13, No. 1, pp. 57-64.

Stewart, M. A., Coccia, C. J. R., and McCartney, J. S., 2014, "Issues in the Implementation of Sustainable Heat Exchange Technologies in Reinforced, Unsaturated Soil Structures," Proceedings of GeoCongress 2014 (GSP 234), M. Abu-Farsakh and L. Hoyos, eds. ASCE. pp. 4066-4075.

Sultan, N., Delage, P. and Cui, Y. J., 2002, "Temperature Effects on the Volume Change Behaviour of Boom Clay," *Engineering Geology*, Vol. 64, pp. 135-145.

Sun, G., Chen, Z. and Liu, Z., 2011, "Analytical and Experimental Investigation of Thermal Expansion Mechanism of Steel Cables," *Journal of Materials in Civil Engineering*, Vol. 23,

No. 7, pp. 1017-1027.

Takai, A., Ghaaowd, I., McCartney, J. S. and Katsumi, T., 2016, "Impact of Drainage Conditions on the Thermal Volume Change of Soft Clay," *Geo-Chicago*, pp. 32-41.

Uchaipichat, A. and Khalili, N., 2009, "Experimental Investigation of Thermo-Hydro-Mechanical Behaviour of an Unsaturated Silt," *Géotechnique*, Vol. 59, No. 4, pp. 339-353.

Vega, A., Coccia, C. J. R., Tawati, A. E. and McCartney, J. S., 2012, " Impact of the Rate of Heating on the Thermal Consolidation of Saturated Silt," *Geo-Congress*, pp. 4476-4485.

Vega, A. and McCartney, J. S., 2015, "Cyclic Heating Effects on Thermal Volume Change of Silt," *Environmental Geotechnics*, Vol. 2, No. 5, pp. 257-268.

Wang, L. Z., Wang, K. J. and Hong, Y., 2016, " Modeling Temperature-Dependent Behavior of Soft Clay," *Journal of Engineering Mechanics*, Vol. 04016054, pp. 1-13.

Wanatowski, D., and Chu, J., 2008, " Effect of Specimen Preparation Method on the Stress-Strain Behavior of Sand in Plane-Strain Compression Tests," *Geotechnical Testing Journal*, Vol. 31, No. 4, pp. 308-320.

Xiao Y., Sun Y. F., Liu H. L., Xiang J., Ma Q. F., and Long L. H., 2017, "Model Predictions for Behaviors of Sand-Nonplastic-Fines Mixtures Using Equivalent-Skeleton Void-Ratio State Index," *Science China Technological Sciences*, Vol. 60, No. 5, pp. 878-892.

Xiao Y., Xiang J., Liu H., and Ma Q., 2017, "Strength-Dilatancy Relation of Sand Containing Non-Plastic Fines," *Géotechnique Letters*, Vol. 7, No. 2, pp. 1-7.

Zhou, C. and Ng, C. W. W., 2016, "Effects of Temperature and Suction on Plastic Deformation of Unsaturated Silt under Cyclic Loads," *Journal of Materials in Civil*

545 *Engineering*, Vol. 04016170, pp. 1-11.

Table Caption List:

Table. 1. Details of the experimental program

Table. 2. Data processing procedures to determine thermal volumetric strain

Table. 3. Values of constants

Table. 1. Details of the experimental program

Number	Mean effective stress p': kPa	Applied temperature T: °C	Initial void ratio e_0	Thermal strain: %	
				ε_a	ε_v
1	50	25	0.372	0.000	0.000
2		35	0.370	-0.043	-0.073
3		45	0.375	-0.086	-0.141
4		55	0.371	-0.133	-0.221
5	100	25	0.376	0.000	0.000
6		35	0.375	-0.042	-0.074
7		45	0.373	-0.086	-0.132
8		55	0.370	-0.136	-0.170
9	200	25	0.375	0.000	0.000
10		35	0.372	-0.049	-0.072
11		45	0.370	-0.092	-0.145
12		55	0.374	-0.138	-0.242

Table. 2. Data processing procedures to determine thermal volumetric strain

T: °C	p': kPa	t: h	ΔV_{dr}: cm^3	ΔV_{de}: cm^3	ΔV_w: cm^3	ΔV_s: cm^3	ΔV: cm^3	ε_v: %
25	50	0	0.000	0.000	0.000	0.000	0.000	0.000
35		3	0.430	0.090	0.816	0.254	-0.730	-0.073
45		6	1.020	0.070	1.852	0.511	-1.413	-0.141
55		9	1.740	0.040	3.146	0.777	-2.223	-0.221
25	100	0	0.000	0.000	0.000	0.000	0.000	0.000
35		3	0.450	0.120	0.818	0.256	-0.743	-0.074
45		6	1.130	0.090	1.850	0.512	-1.323	-0.132
55		9	2.260	0.060	3.133	0.776	-1.709	-0.170
25	200	0	0.000	0.000	0.000	0.000	0.000	0.000
35		3	0.420	0.080	0.810	0.254	-0.724	-0.072
45		6	0.950	0.060	1.832	0.510	-1.452	-0.145
55		9	1.530	0.040	3.131	0.779	-2.420	-0.242

Table. 3. Values of constants

Equation number	Symbol	Unit	Value
(6)	χ_{io}	°C	-0.094
	k_{io}	-	0.020
(7)	χ_{bt}	°C	1.519
	k_{bt}	-	-0.024
(9)	k_{at}	-	-0.112
(10)	k_{vt}	-	-0.176
(11)	k_{av}	-	0.628
(12)	β	%/°C	-0.007
(13)	a		0.017
	b		-0.021
(14)	c		0.006
	d		-0.003

Figure Caption List:

Fig. 1. Photo of the temperature-controlled hollow triaxial apparatus

Fig. 2. Schematic diagram of the temperature-controlled hollow triaxial apparatus

Fig. 3. Particle size distribution for Fujian sand

Fig. 4. Stress paths for Fujian sand

Fig. 5. Axial displacement of the dummy sample during the heating-cooling cycle

Fig. 6. Volume change of drainage system during the heating-cooling cycle

Fig. 7. Time series of temperature and water volume expelled from specimen (p'=50 kPa)

Fig. 8. Time series of temperature of the sand specimen during the staged heating phases performed under a mean effective stress of p'=50 kPa: (a) Temperatures on the inside (inner) and outside (cell) of the specimen; (b) Temperatures at the top and bottom of the cell

Fig. 9. Differences in the spatial distribution in temperature in the specimen during heating to different target temperatures (p'=50 kPa)

Fig. 10. Time series of axial and volumetric strains (p'=50 kPa)

Fig. 11. Typical time series of the consist of the thermal volumetric strain (p'=50 kPa)

Fig. 12. Relationship between the thermal axial strain and temperature ratio

Fig. 13. Relationship between the thermal volumetric strain and temperature ratio

Fig. 14. Relationship between the thermal axial and volumetric strains

Fig. 15. Relationship between the thermal volumetric strain and temperature change

with the bulk thermal expansion coefficient of sand specimen

Fig. 16. (a) Relationship between the bulk thermal expansion coefficient and relative densities for Toyoura sand (data from Ng et al. 2016) and Fujian sand; (b) Relationship between the bulk thermal expansion coefficient and overconsolidation ratio for Kaolin clay (data from Cekerevac and Laloui 2004)

Fig. 17. Change in relative density of the sand specimen before and after mechanical consolidation

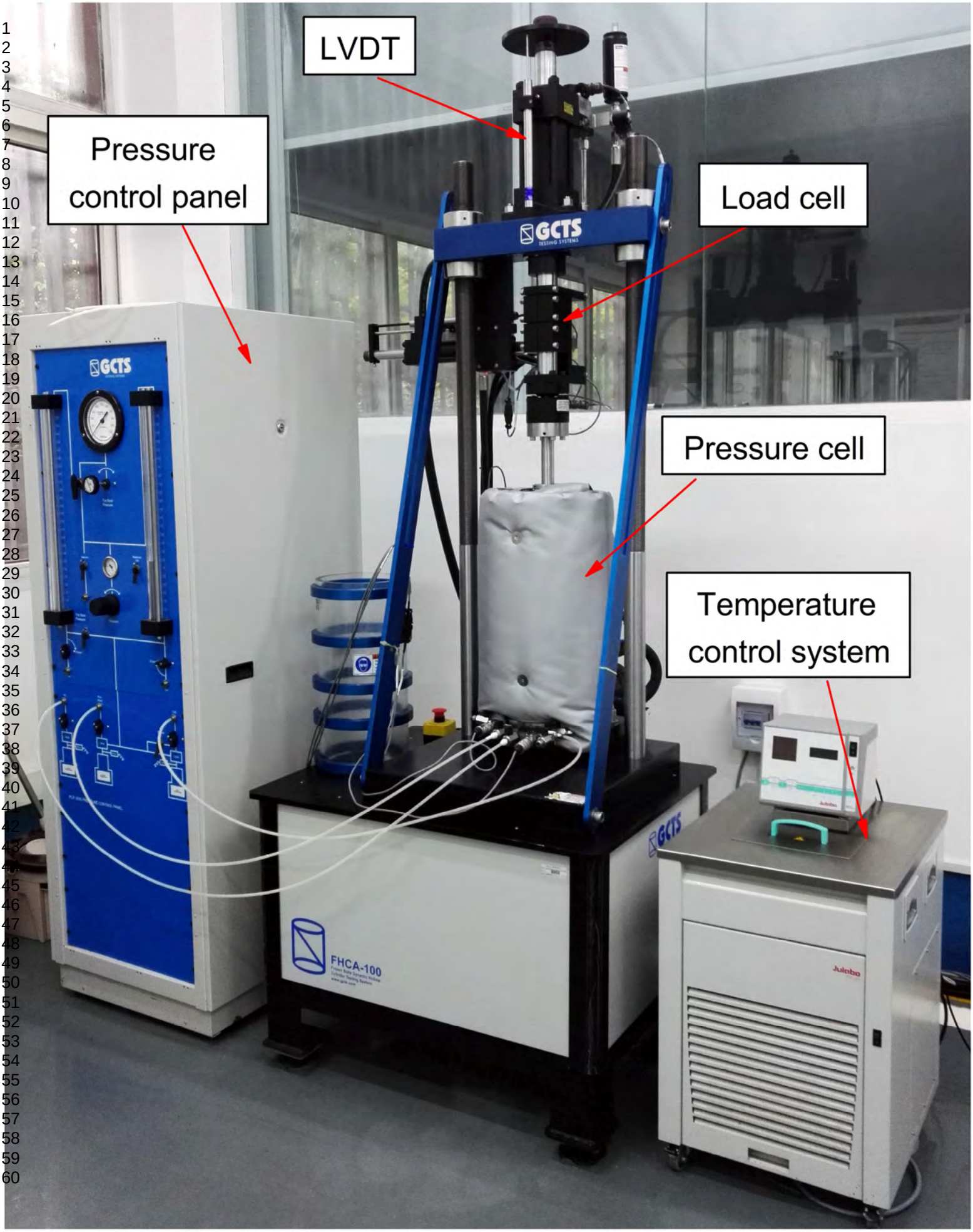
LVDT
Pressure control panel
Load cell
Pressure cell
Temperature control system
GCTS
FHCA-100
Julabo

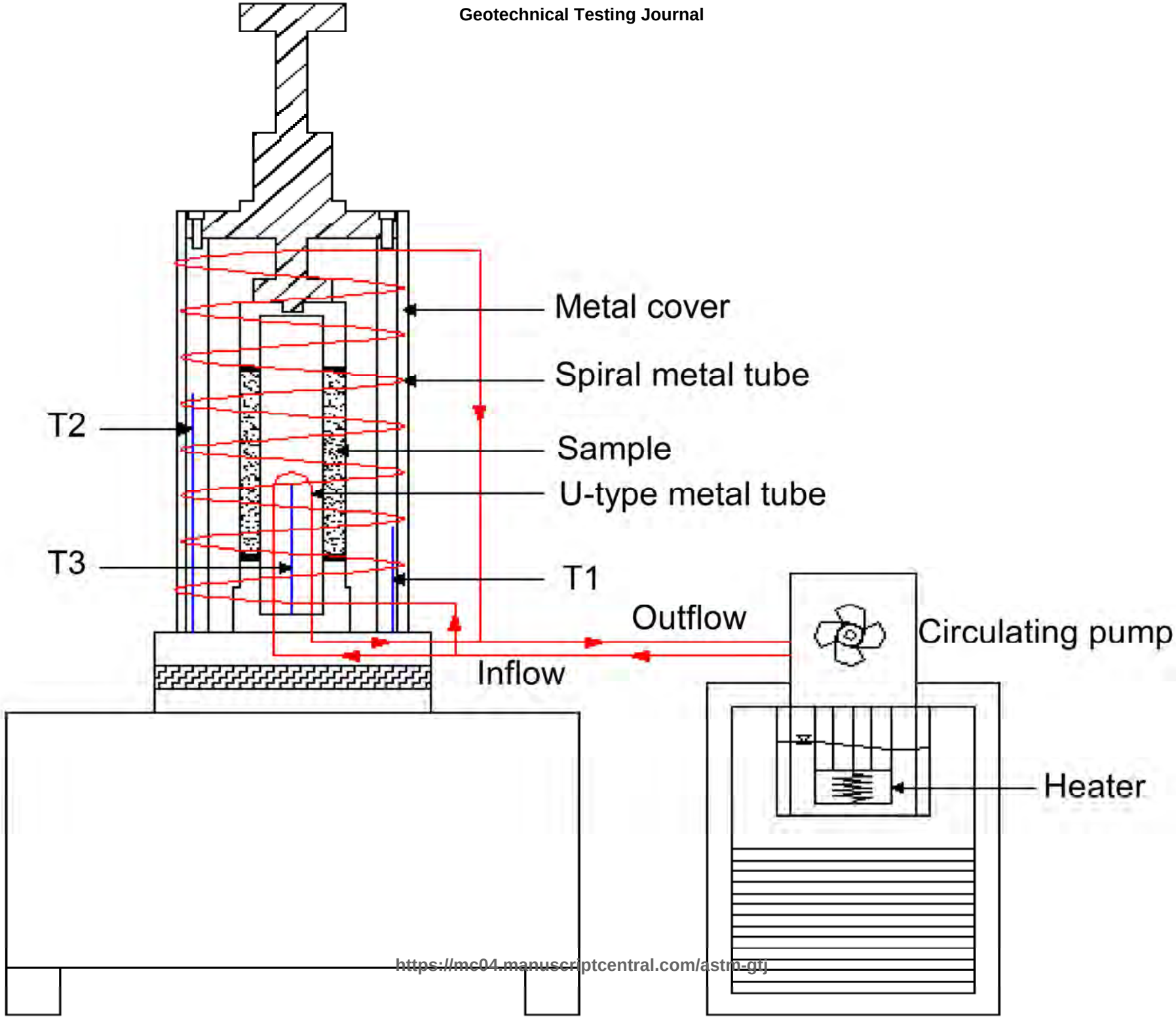

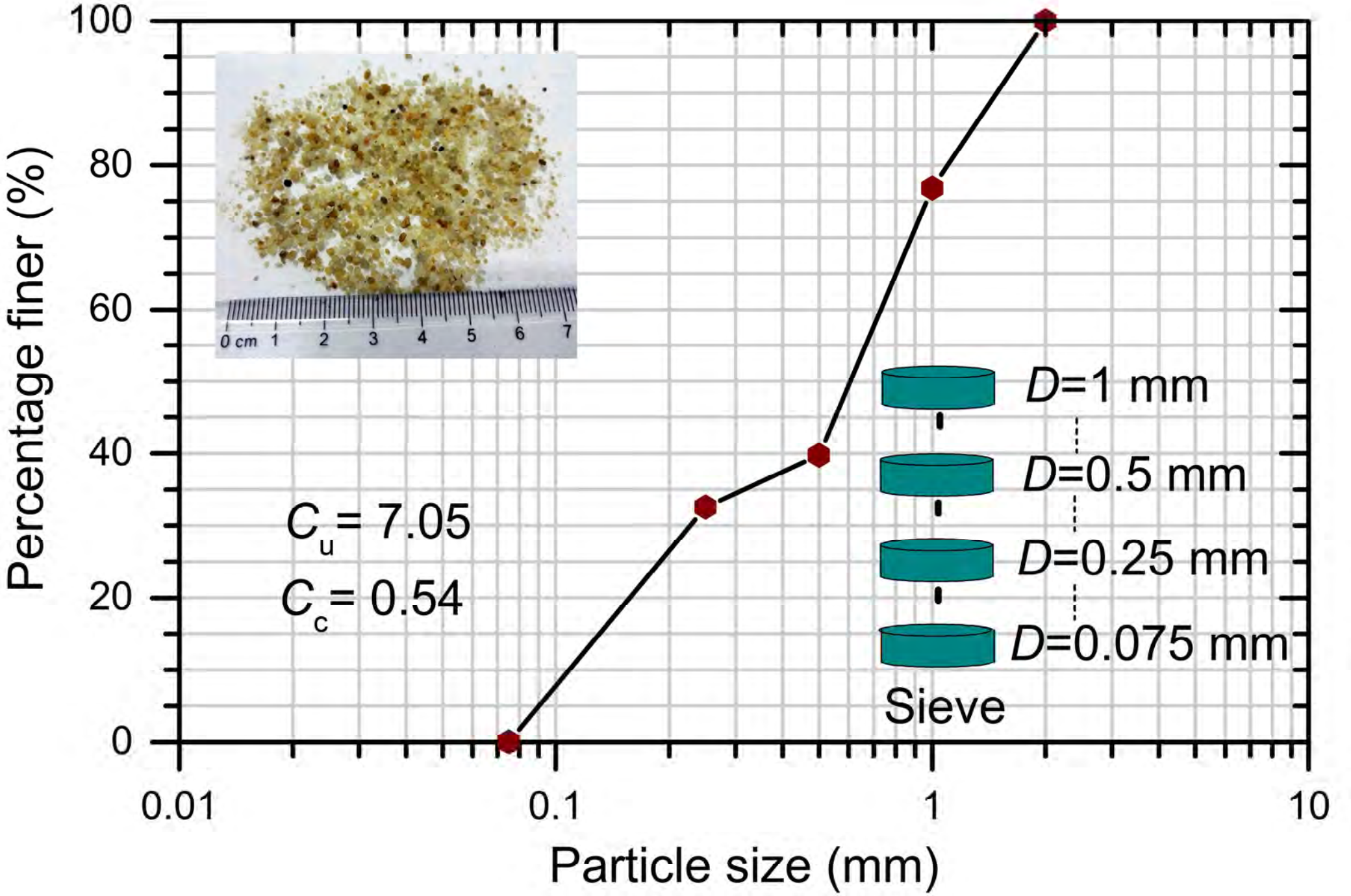
100
80
60
40
20
0
Percentage finer (%)
0.01
0.1
1
10
Particle size (mm)
0 cm 1 2 3 4 5 6 7
C_u = 7.05
C_c = 0.54
D=1 mm
D=0.5 mm
D=0.25 mm
D=0.075 mm
Sieve

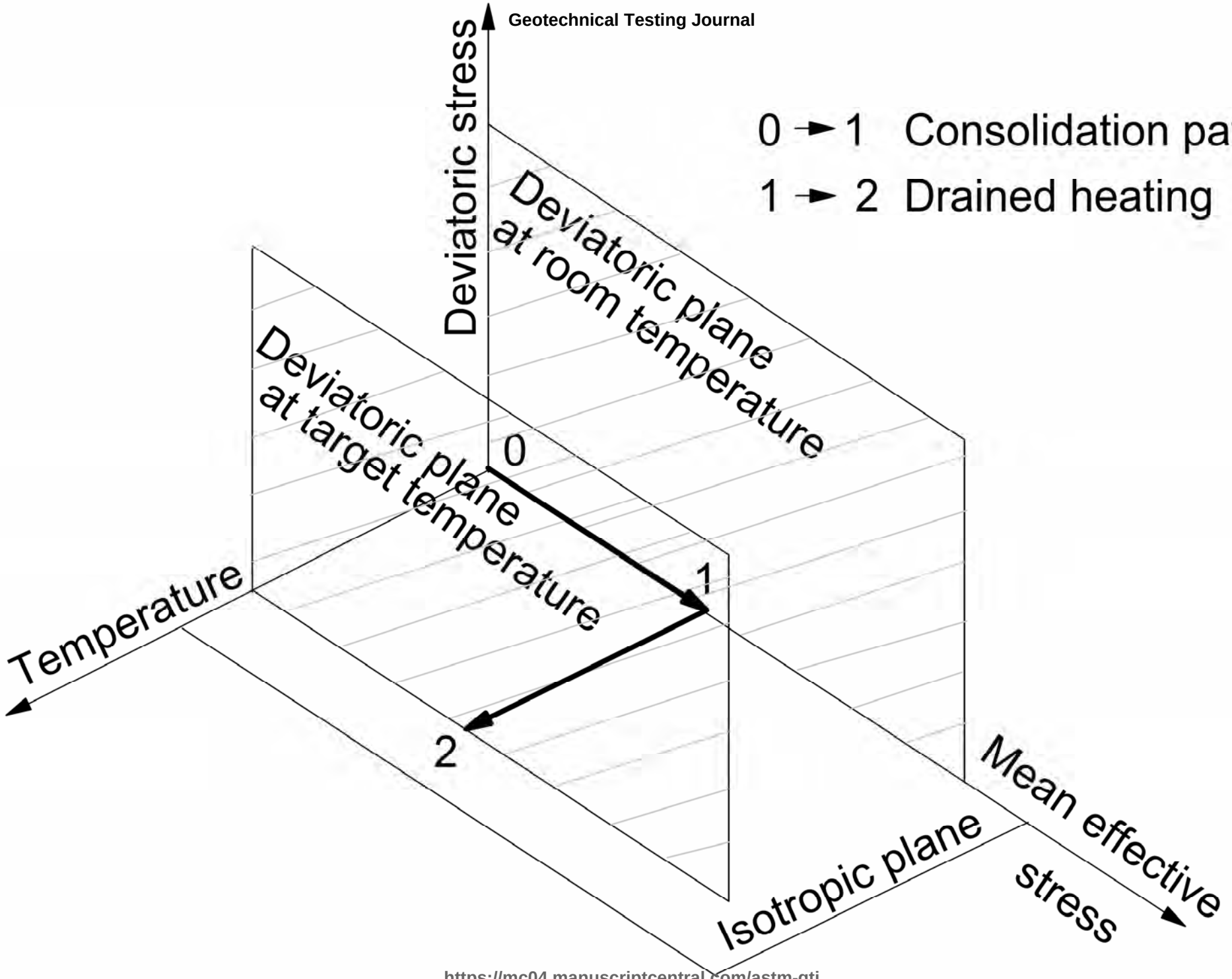
Deviatoric stress
0 → 1 Consolidation path
1 → 2 Drained heating
Deviatoric plane at room temperature
Deviatoric plane at target temperature
0
1
2
Temperature
Isotropic plane
Mean effective stress

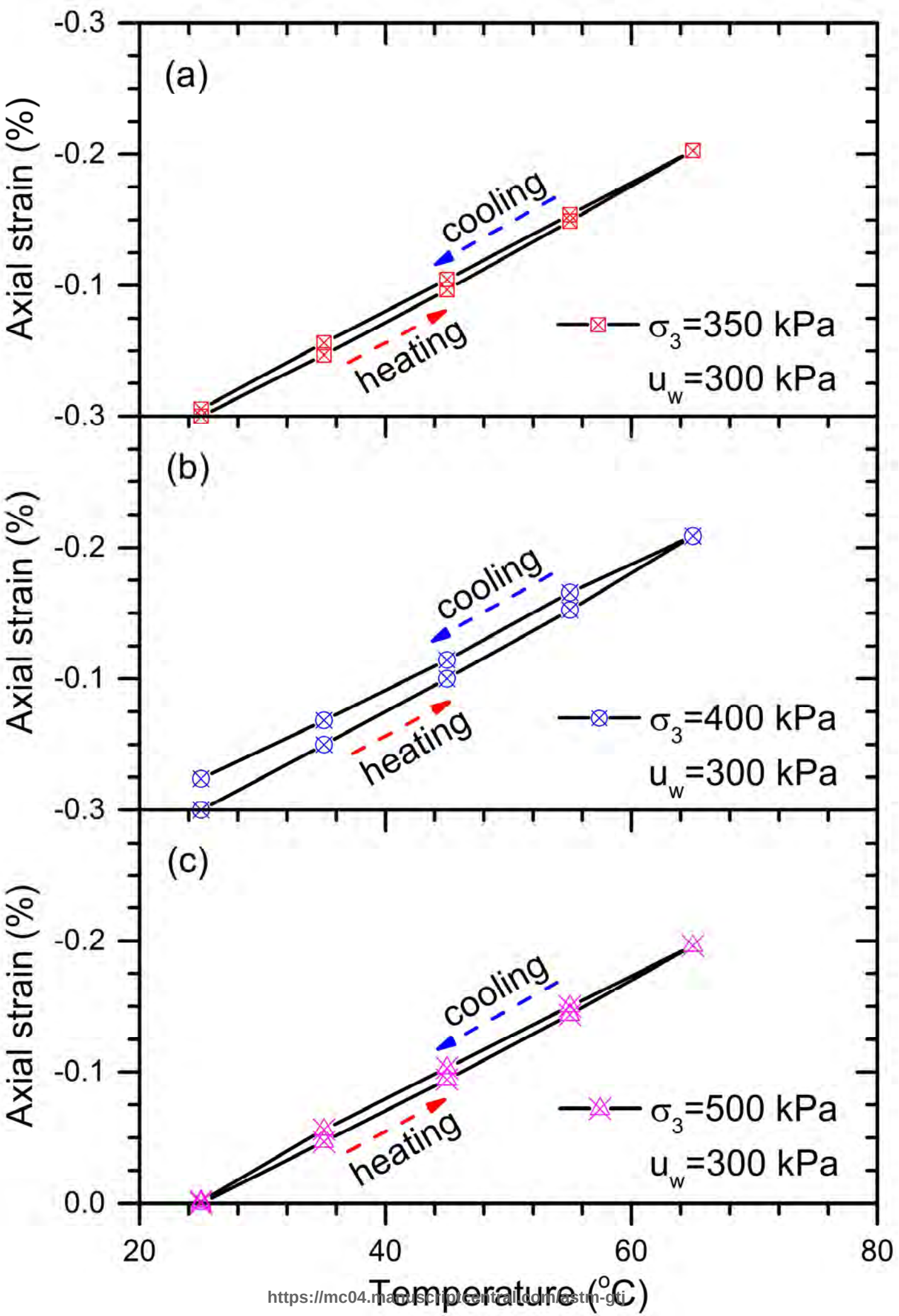

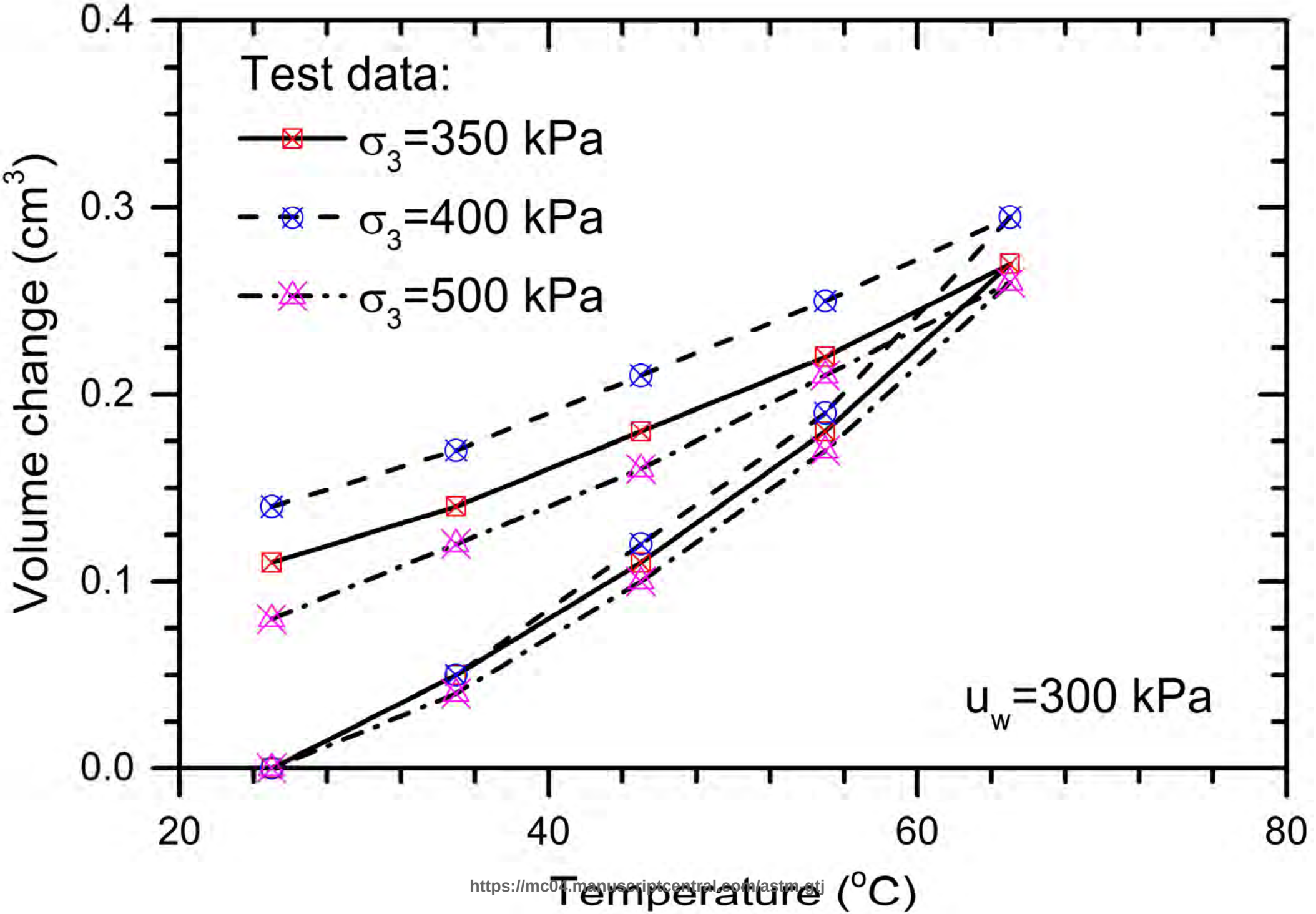

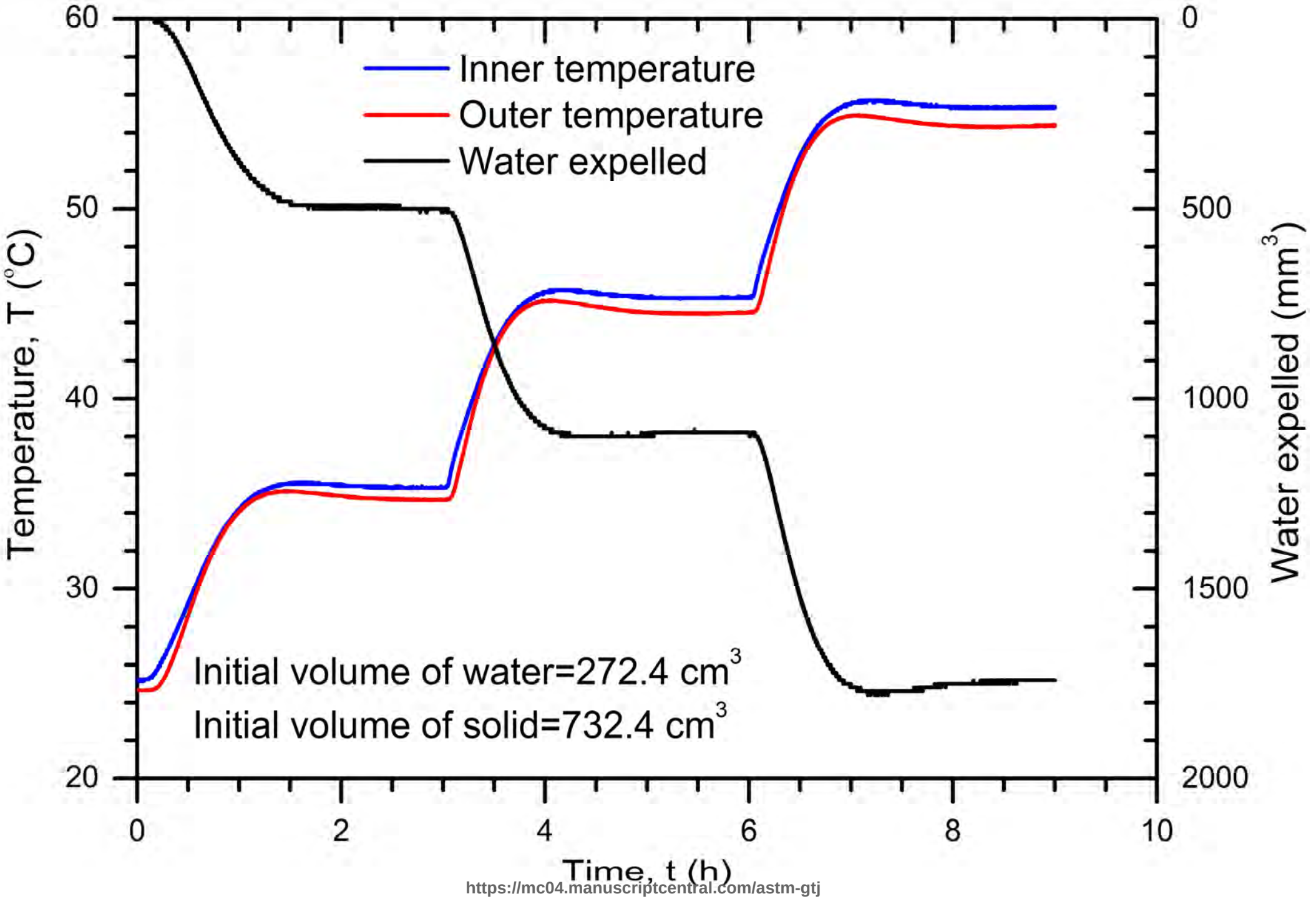
Inner temperature
Outer temperature
Water expelled
Initial volume of water=272.4 cm3
Initial volume of solid=732.4 cm3
Temperature, T (°C)
Water expelled (mm3)
Time, t (h)
60
50
40
30
20
0
500
1000
1500
2000
0
2
4
6
8
10

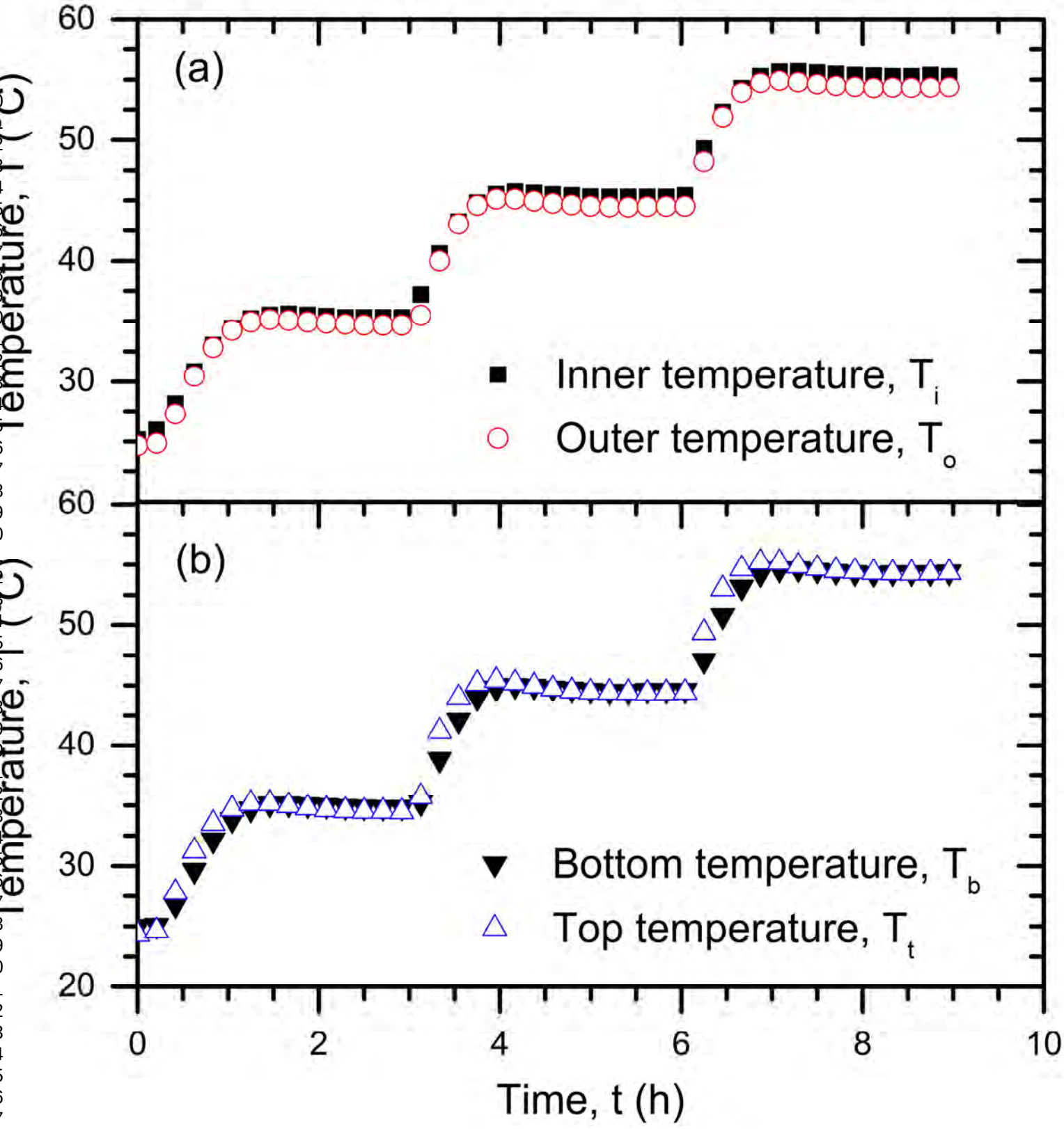
(a)
Temperature, T (°C)
60
50
40
30
Inner temperature, T_i
Outer temperature, T_o
(b)
Temperature, T (°C)
60
50
40
30
20
Bottom temperature, T_b
Top temperature, T_t
0
2
4
6
8
10
Time, t (h)

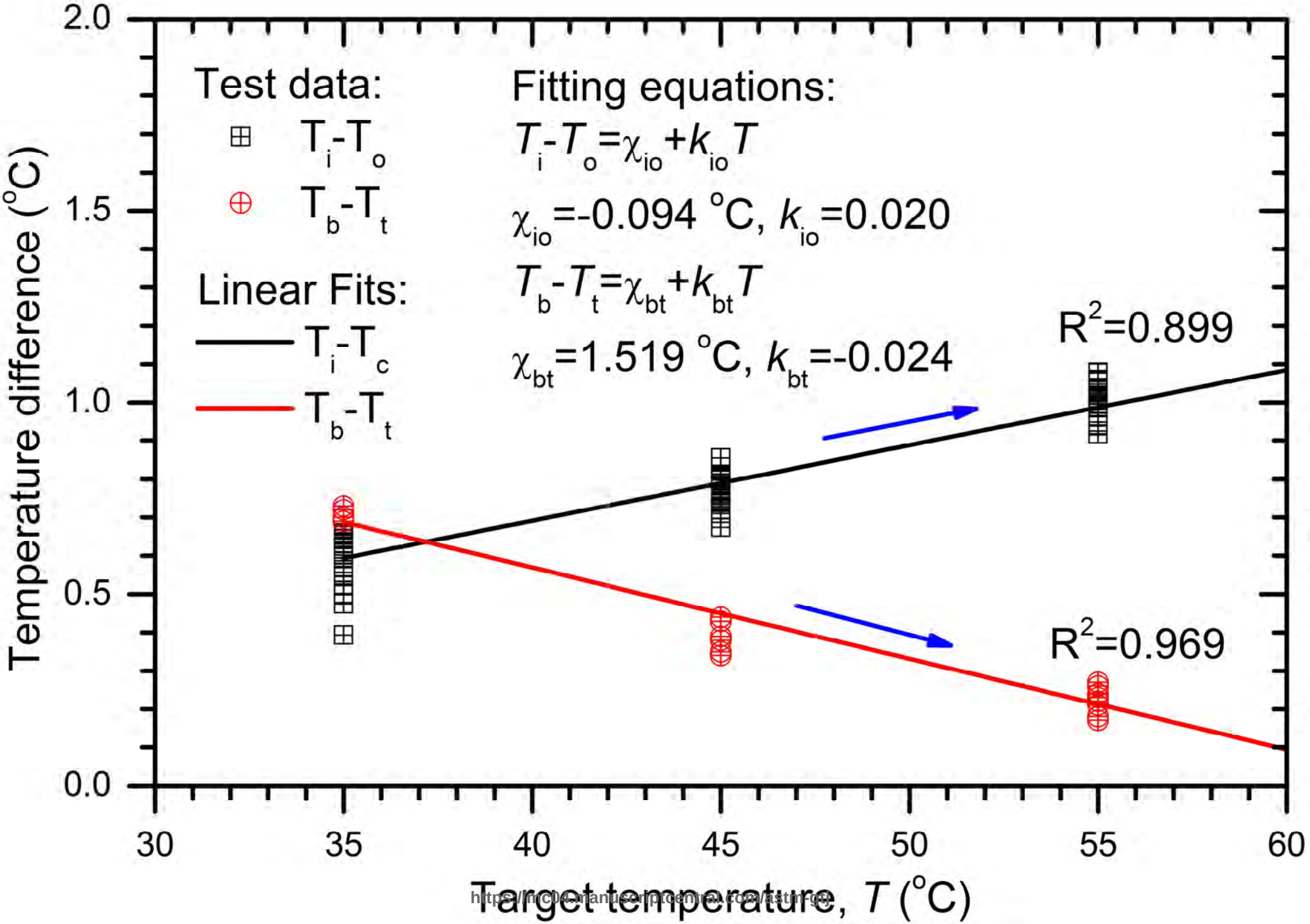

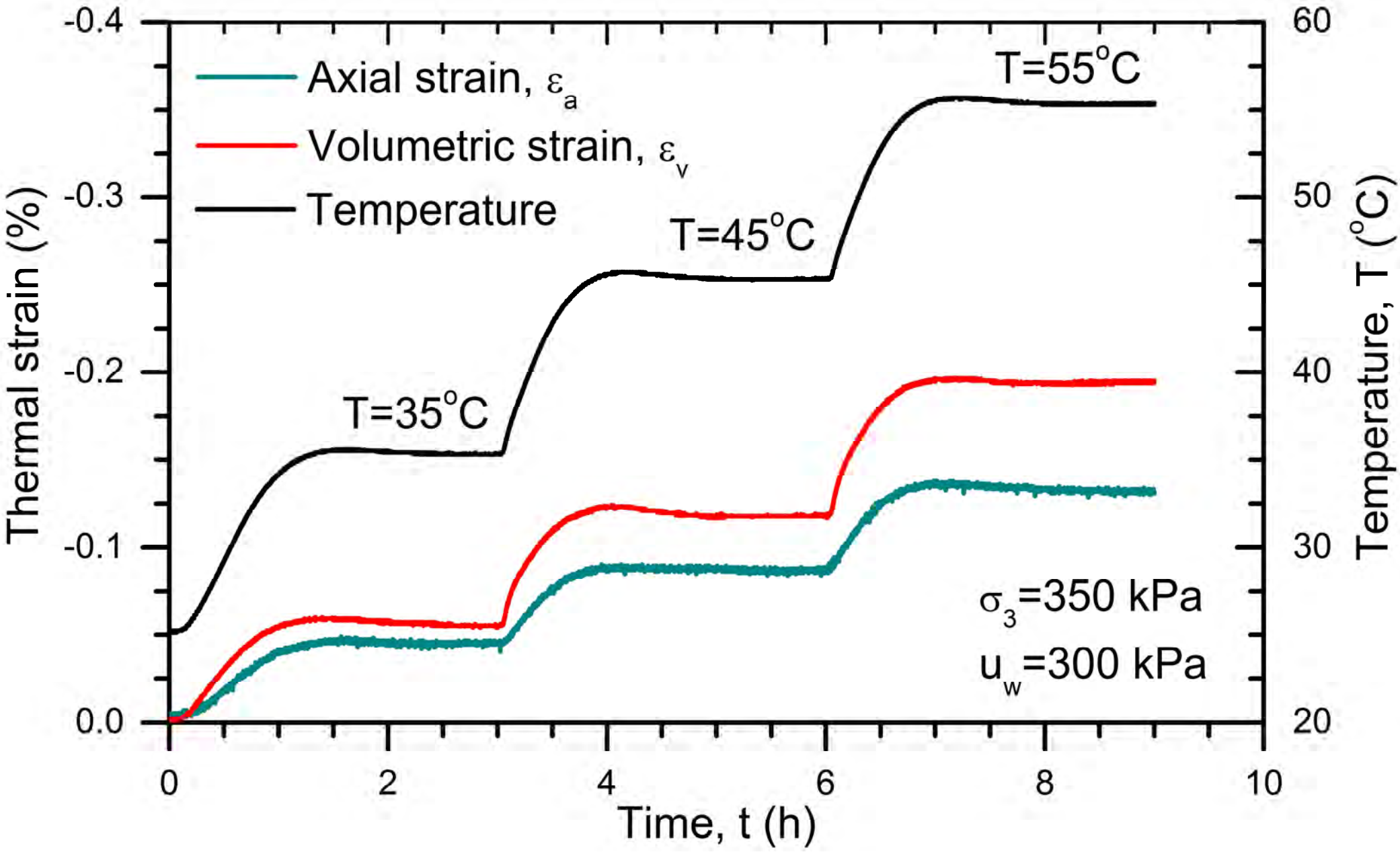
Axial strain, ε_a
Volumetric strain, ε_v
Temperature
T=35°C
T=45°C
T=55°C
σ_3=350 kPa
u_w=300 kPa
Thermal strain (%)
Temperature, T (°C)
Time, t (h)
-0.4
-0.3
-0.2
-0.1
0.0
60
50
40
30
20
0
2
4
6
8
10

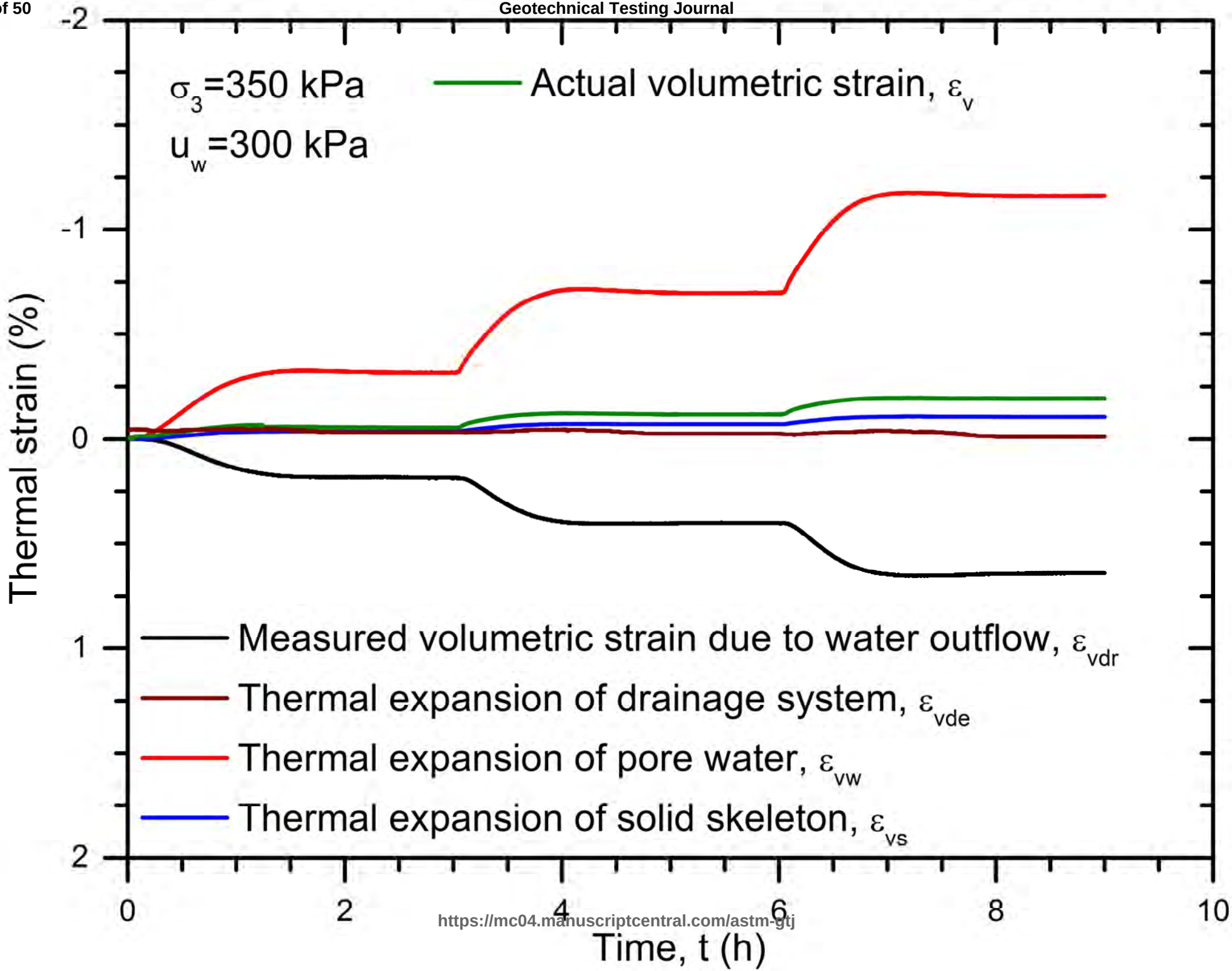
σ3=350 kPa
uw=300 kPa
Actual volumetric strain, εv
Thermal strain (%)
-2
-1
0
1
2
Measured volumetric strain due to water outflow, εvdr
Thermal expansion of drainage system, εvde
Thermal expansion of pore water, εvw
Thermal expansion of solid skeleton, εvs
0
2
4
6
8
10
Time, t (h)

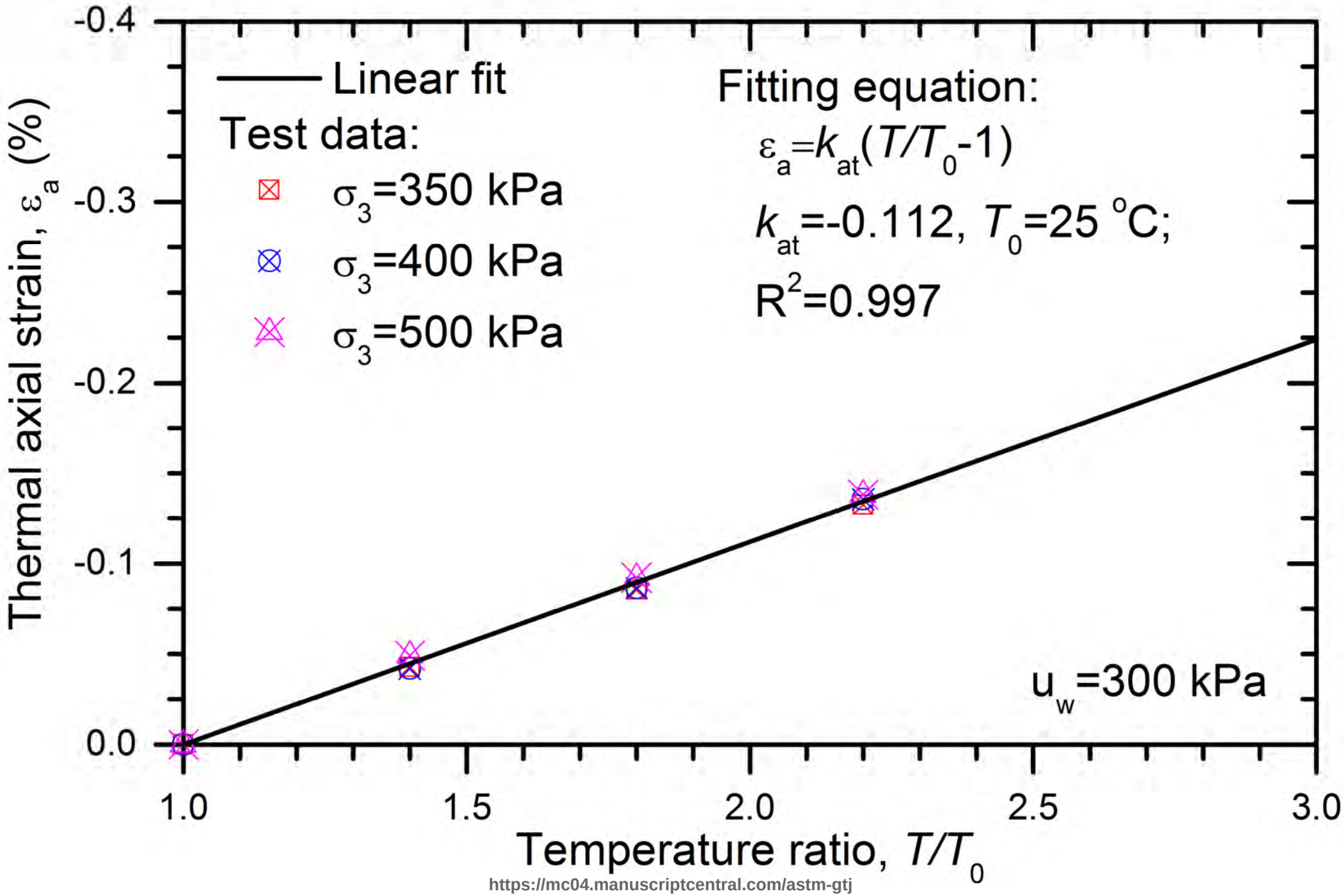
Linear fit
Test data:
σ3=350 kPa
σ3=400 kPa
σ3=500 kPa
Fitting equation:
εa=kat(T/T0-1)
kat=-0.112, T0=25 °C;
R2=0.997
uw=300 kPa
Thermal axial strain, εa (%)
-0.4
-0.3
-0.2
-0.1
0.0
1.0
1.5
2.0
2.5
3.0
Temperature ratio, T/T0

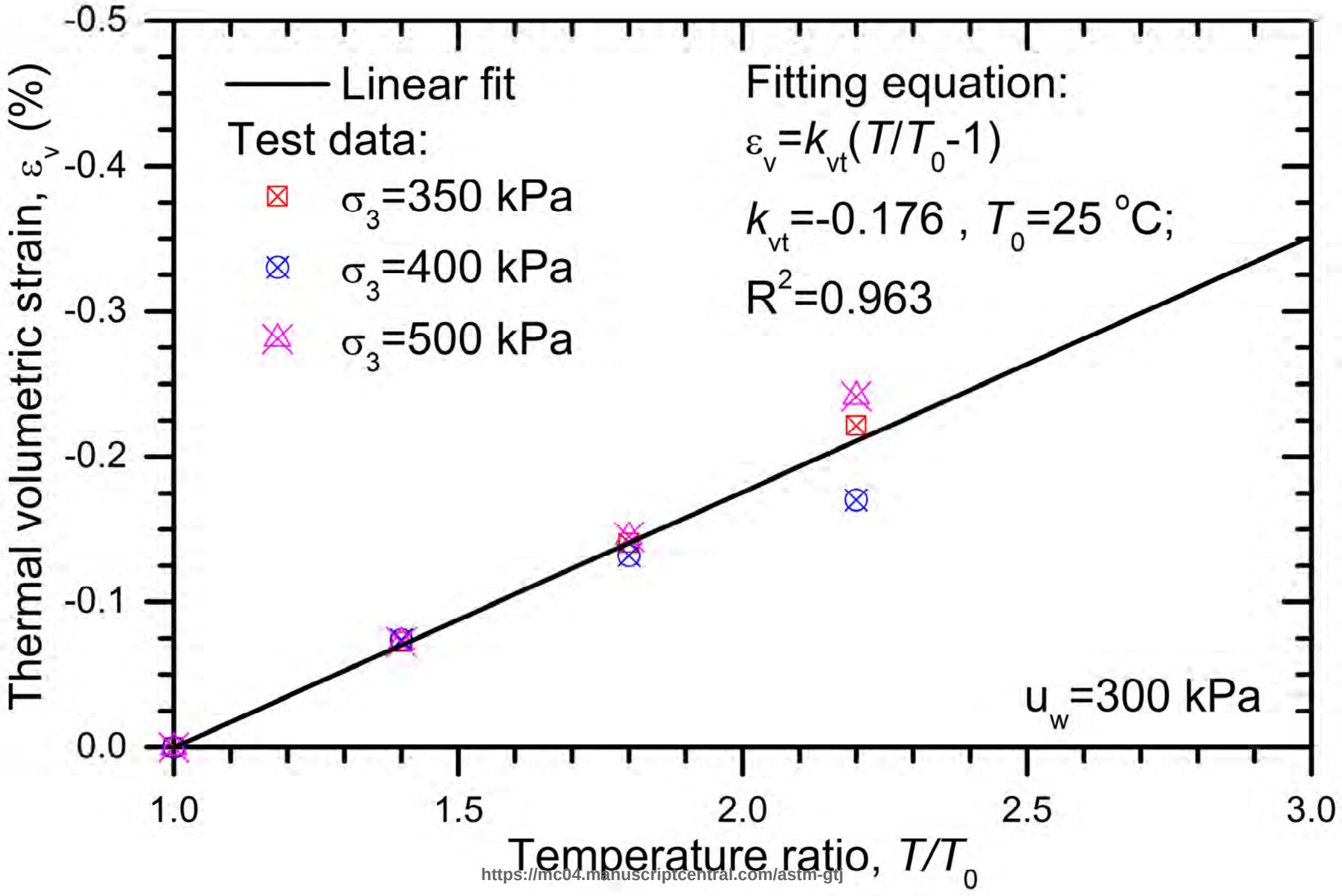
Linear fit
Test data:
σ3=350 kPa
σ3=400 kPa
σ3=500 kPa
Fitting equation:
εv=kvt(T/T0-1)
kvt=-0.176 , T0=25 °C;
R2=0.963
uw=300 kPa
Thermal volumetric strain, εv (%)
-0.5
-0.4
-0.3
-0.2
-0.1
0.0
1.0
1.5
2.0
2.5
3.0
Temperature ratio, T/T0

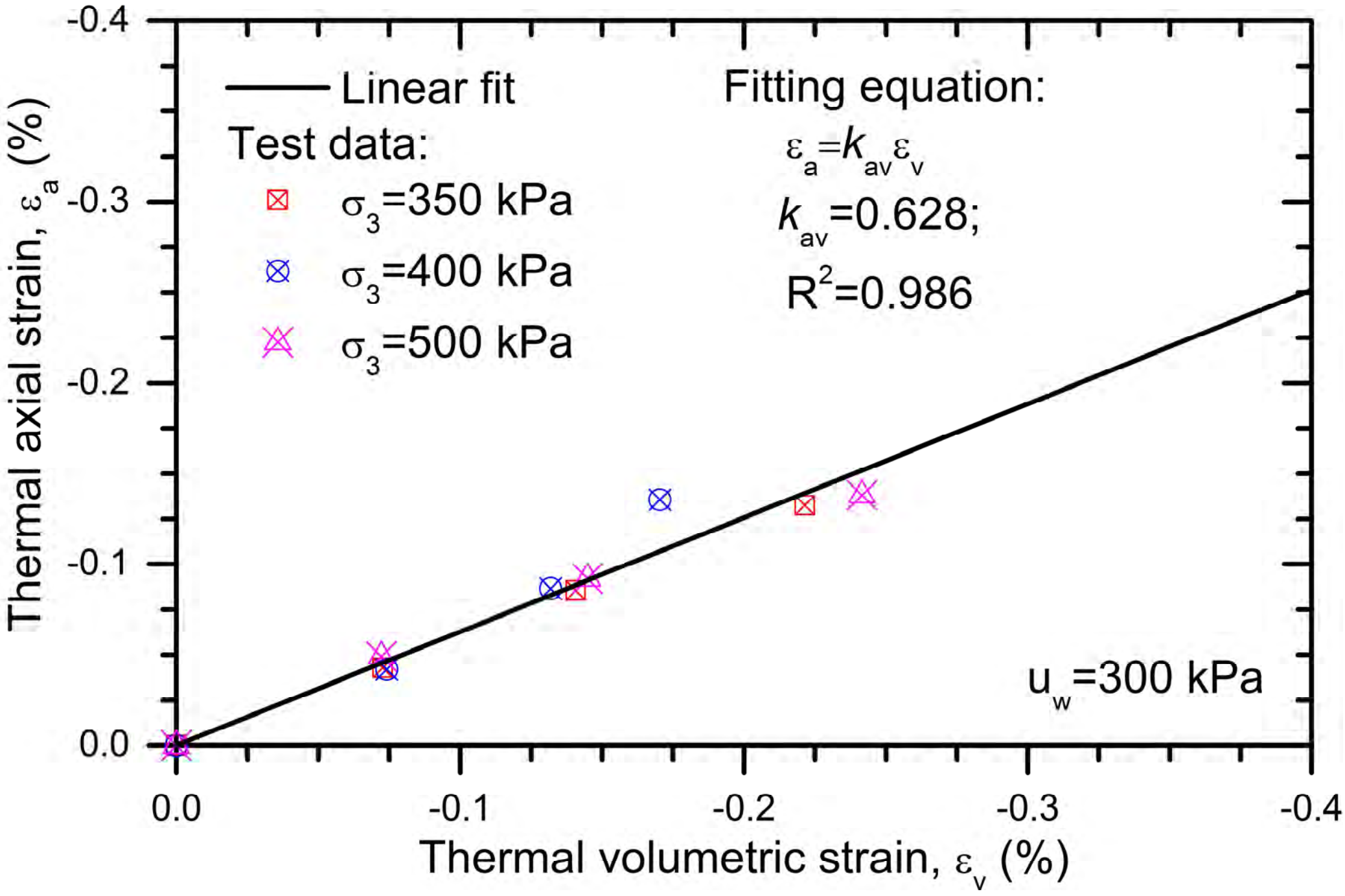
Linear fit
Test data:
σ3=350 kPa
σ3=400 kPa
σ3=500 kPa
Fitting equation:
εa=kav εv
kav=0.628;
R2=0.986
uw=300 kPa
Thermal axial strain, εa (%)
Thermal volumetric strain, εv (%)
-0.4
-0.3
-0.2
-0.1
0.0

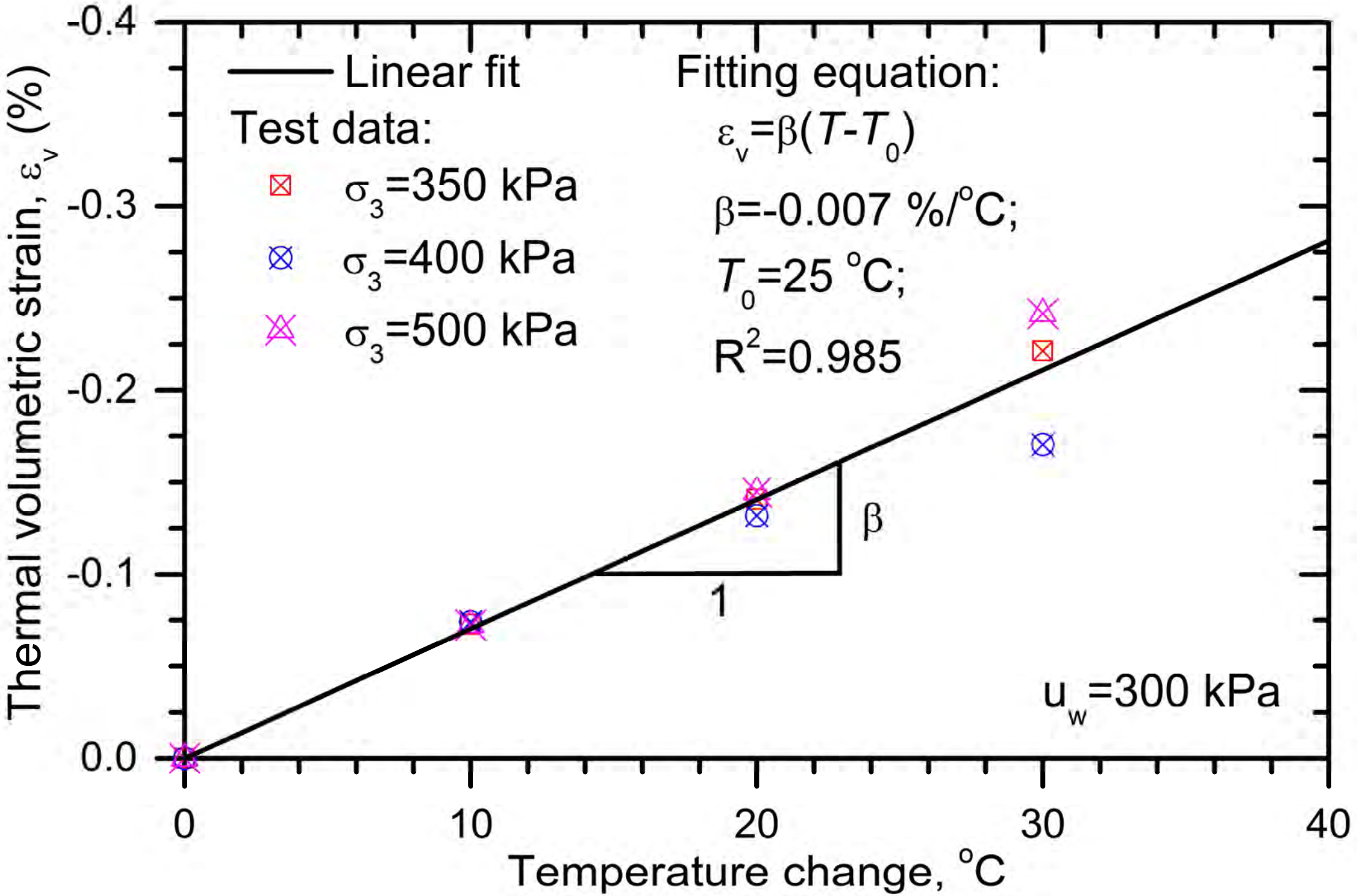
Linear fit
Test data:
σ3=350 kPa
σ3=400 kPa
σ3=500 kPa
Fitting equation:
εv=β(T-T0)
β=-0.007 %/°C;
T0=25 °C;
R2=0.985
β
1
uw=300 kPa
Thermal volumetric strain, εv (%)
Temperature change, °C
-0.4
-0.3
-0.2
-0.1
0.0
0
10
20
30
40

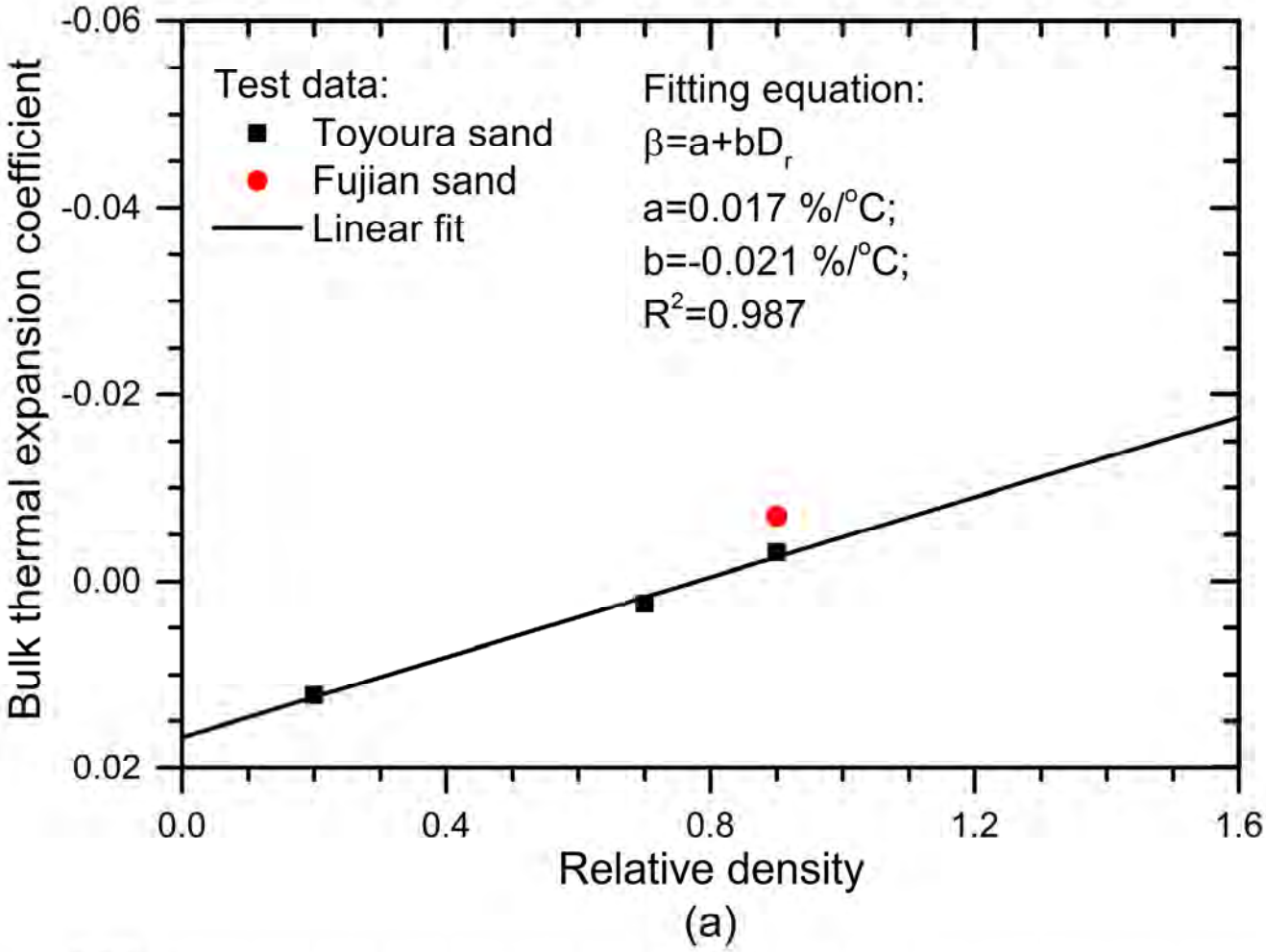
Test data:
Toyoura sand
Fujian sand
Linear fit
Fitting equation:
β=a+bD_r
a=0.017 %/°C;
b=-0.021 %/°C;
R²=0.987
Bulk thermal expansion coefficient
-0.06
-0.04
-0.02
0.00
0.02
0.0
0.4
0.8
1.2
1.6
Relative density

(a)

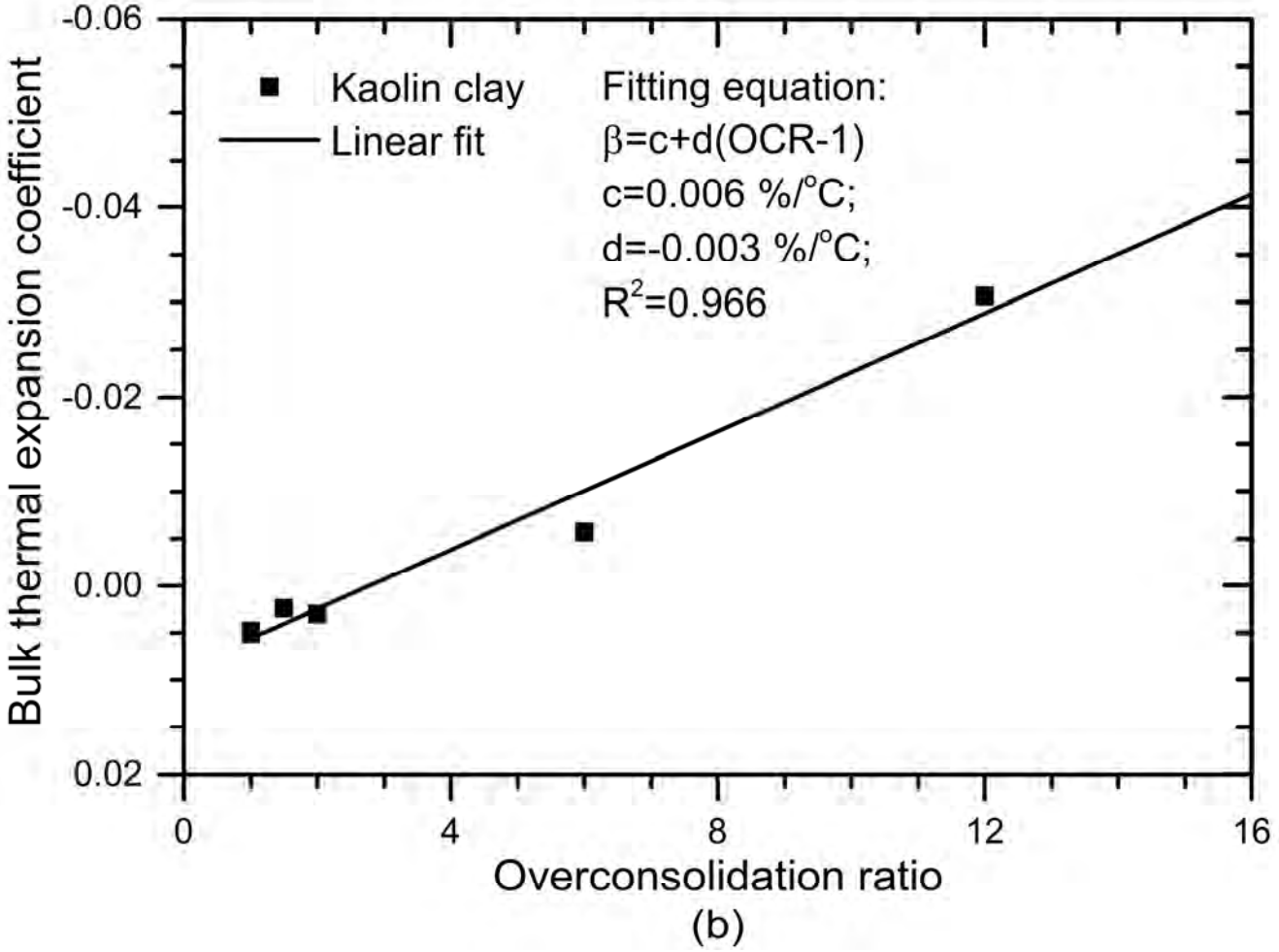
Kaolin clay
Linear fit
Fitting equation:
β=c+d(OCR-1)
c=0.006 %/°C;
d=-0.003 %/°C;
R²=0.966
Bulk thermal expansion coefficient
-0.06
-0.04
-0.02
0.00
0.02
0
4
8
12
16
Overconsolidation ratio

(b)

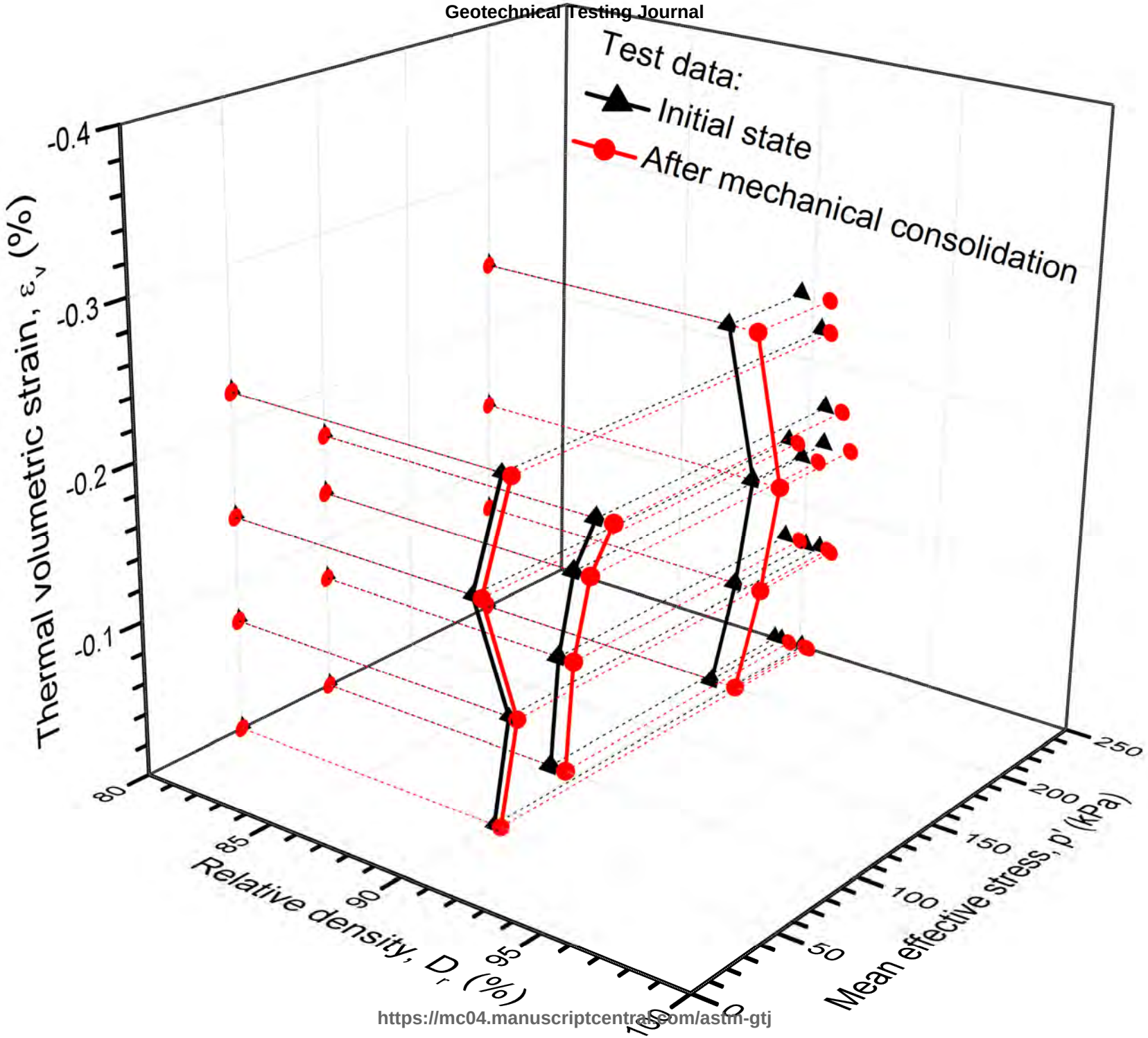
Test data:
Initial state
After mechanical consolidation
Thermal volumetric strain, ε_v (%)
-0.4
-0.3
-0.2
-0.1
0
Relative density, D_r (%)
80
85
90
95
100
Mean effective stress, p' (kPa)
0
50
100
150
200
250